Ore Geology Reviews 131 (2021) 104061

Contents lists available at ScienceDirect

Ore Geology Reviews

journal homepage: www.elsevier.com/locate/oregeorev

Multivariate statistical analysis of trace element compositions of native gold from orogenic gold deposits: Implication for mineral exploration

Haiming Liu [a,b,*], Georges Beaudoin [a,b], Sheida Makvandi [a], Simon E. Jackson [c], Xiaowen Huang [a,b,d]

[a] Département de géologie et de génie géologique, Université Laval, Québec G1V 0A6, Canada
[b] Research Center on the Geology and Engineering of Mineral Resources (E4M), Université Laval, Québec G1V 0A6, Canada
[c] Natural Resources Canada, Ottawa K1A 0E8, Canada
[d] State Key Laboratory of Ore Deposit Geochemistry, Institute of Geochemistry, Chinese Academy of Sciences, Guiyang 550081, China

ARTICLE INFO

Keywords:
Orogenic gold deposit
Geochemical composition
Native gold
Partial least squares discriminant analysis
EPMA
LA-ICP-MS

ABSTRACT

The mineralogy and chemical composition of native gold from twenty-seven representative orogenic gold deposits were investigated using optical microscopy, electron probe microanalysis (EPMA), and laser ablation-inductively coupled plasma-mass spectrometry (LA-ICP-MS). Minor elements, such as Ag and Cu, occur in solid solution, while trace elements, such as Fe, As, S, Hg, form impurities or micro inclusions in native gold. Partial least squares-discriminant analysis (PLS-DA) has identified compositional characteristics based on mineral association, gold texture and dominant country rocks. Gold grains are commonly associated with pyrite, arsenopyrite, chalcopyrite, pyrrhotite, and tourmaline in the studied orogenic deposits. Chemical variations in gold with different associated mineral assemblages are related to the partitioning of trace elements between co-crystalizing minerals and gold during precipitation. Gold inclusions in gangue minerals are discriminated from later gold in fractures based on contents of Ag, Fe, Pb, and Bi, which indicates that gold in different paragenetic stages of mineralization can be identified using its trace element signature. Gold hosted in different regional country rocks can be discriminated by Ag, Cu, Pd, Sb, and Hg, likely because of reactions of hydrothermal fluids with the regional country rocks along the fluid flow paths.

1. Introduction

Indicator minerals can indicate the presence of a specific mineral deposit, alteration type, or rock lithology (McClenaghan, 2011). The application of indicator mineral methods using garnet, magnetite, Cr diopside, olivine, gold, etc., to mineral exploration has developed significantly over the past three decades. Indicator minerals are now used to explore for various deposit types, such as porphyry Cu, lode gold, magmatic Ni-Cu-PGE, volcanogenic massive sulfide, rare earth, diamond, and iron oxide-copper-gold deposits (McClenaghan, 2005; McClenaghan and Layton-Matthews, 2017; Cooke et al., 2020).

Native gold occurs in a variety of deposit types and the chemical composition of the gold can be associated with a wide range of transport media and precipitation processes (Chapman et al., 2009; Frimmel, 2014). Thus, native gold may possess a geochemical signature related to a specific deposit type, which could be used to identify the source of detrital gold found in overburden sediments.

Native gold is an alloy of Au and Ag, with minor Cu, S and Hg, in proportions that vary with the conditions of formation (Desborough, 1970; Boyle, 1979). Gold compositions have been measured by electron probe microanalysis (EPMA) for Ag, Cu, and Hg in several deposit types (Chapman et al., 2010a, 2011, 2017; Omang et al., 2015; Mehrabi et al., 2019). Combining alloy compositions and inclusion mineralogy allowed identification of various alloy types for placer gold derived from deposits that were precipitated by highly oxidized chloride hydrothermal systems based on the relative proportions of Au, Ag, Pd and Hg (Chapman et al., 2009). Detrital gold grains from porphyry deposits from Yukon (Canada), characterized by a Bi-Pb-Te-S inclusion suite mineralogy, typically exhibits a slightly higher Cu content compared to gold from epithermal deposits, which shows a wide range of Au/Ag ratios from different deposits but a relatively narrow Ag range from individual deposits (Morrison et al., 1991; Chapman et al., 2018). Based on the contents of Au, Ag and Cu, ternary diagrams were constructed to distinguish gold from porphyry Cu, porphyry Cu-Au, and epithermal

* Corresponding author.
E-mail address: haimingliu1989@gmail.com (H. Liu).

https://doi.org/10.1016/j.oregeorev.2021.104061
Received 25 May 2020; Received in revised form 25 November 2020; Accepted 17 January 2021
Available online 11 February 2021

deposits (Townley et al., 2003). However, due to the limited numbers of elements measured (Au, Ag, Cu, Hg, Fe), these diagrams are not able to differentiate gold from epithermal and orogenic gold deposits (Moles et al., 2013).

Analysis of gold grains by LA-ICP-MS for elements such as Mo, Sb, and Sn allowed fingerprinting of groups of gold grains or deposits from Western Australia and South Africa (Watling et al., 1994). The trace element composition of gold grains from the Klondike District (Canada) suggests that Pt, Sn, Hg, Cu, Cd, and As variations can be used to discriminate different placer gold subgroups (Crawford, 2007). Velasquez (2014) reported 64 trace element analyses from the Hollinger, Mclntyre, and Aunor orogenic deposits (Canada) by LA-ICP-MS and suggested that chalcophile (Ag, Cu, Zn, Bi, Sb, Pb, As, and Sn) and siderophile elements (Pd, Fe, Co, Ni, and Mo) fingerprint these orogenic gold deposits, whereas lithophile (Mg, Al, Ca, Si, and Ti) elements are not useful for distinguishing these orogenic gold deposits from other deposit types. A large suite of elements determined by LA-ICP-MS and EPMA has been used to identify the Au-Ag-Cu-Hg-Sb signatures of around 800 detrital gold grains derived from orogenic and alkalic porphyry deposits from 18 different localities in British Columbia(Canada, Banks et al., 2018). However, most previous studies focused on the chemical compositions of placer gold in specific regional localities which are not sufficient to build relationship between the geochemical signatures of native gold and generic characteristics in orogenic deposits. The chemical data in this study are derived from economically important orogenic gold deposits worldwide, which can be used to compare with previous studies.

Orogenic gold deposits are the source of 75% of the world's gold production (Goldfarb et al., 2001; Goldfarb and Groves, 2015; Gaboury, 2019). Orogenic gold deposits dominantly occur in metamorphic rocks that formed in the mid- to shallow crust (5–15 km depth), at or above the brittle-ductile transition, in compressional settings that facilitate transport of Au-bearing fluids from deep levels in the crust (Groves et al., 2003; Goldfarb et al., 2005; Goldfarb and Groves, 2015). Alternatively, multistage fluids during the late diagenesis and metamorphism may play a key role in upgrading gold grade to form large orogenic deposits in active continental margin settings (Large et al., 2007; Meffre et al., 2016; Augustin and Gaboury, 2019). Native gold in orogenic gold deposits is dominantly found in quartz-carbonate veins as well as in biotite- or actinolite-altered and schistose wall rocks. Most of the gold occurs as fine grains along quartz or sulfide boundaries and in fractures, and as isolated inclusions within pyrite (Goldfarb et al., 2005). Gold can also be associated with tourmaline, tellurides and carbonate veins (Dubé and Gosselin, 2007; Tshibubudze and Hein, 2016; Kalliomäki et al., 2017). The concentration of trace elements in gold likely depends on (1) the concentration of the trace element in the fluids, (2) the partition coefficient of the element between native gold and co-existing minerals, (3) physicochemical conditions of fluids, such as temperature, pressure, oxygen fugacity, and (4) the ionic radii of trace element in Au-Ag alloy (Hough et al., 2009; Garofalo et al., 2014; Wyman et al., 2016; Pokrovski et al., 2019).

The aim of this study is to characterize the chemical compositions of native gold in orogenic systems and to discuss the controls of the trace element distributions in native gold grains. In order to identify systematic differences in gold grain composition, we used in situ analytical techniques to investigate the major and trace element compositions of gold from representative orogenic gold deposits located in various geological settings, with ages ranging from the Archean to the Cretaceous. Statistical interrogation of the gold composition dataset is then used to examine the potential control of mineral association, texture, and dominant country rocks on the variations of gold composition in orogenic gold deposits.

2. Samples and analytical methods

2.1. Sample collection

A total of 287 native gold grains were investigated from twenty-seven orogenic deposits or districts worldwide (Fig. 1). The deposits selected for this study are documented as orogenic gold deposits in literature, and for which adequate background information exists. The samples come from different orogens, with a wide variety of mineralization ages from the Archean to the Cretaceous and are hosted by various types of country rocks including ultramafic to mafic, intermediate and felsic igneous rocks, and sedimentary rocks (Table 1). The host rocks were metamorphosed from the greenschist to the granulite grade. The need for a broad scope of gold samples is to capture the variance that may arise from different compositions of gold grains resulting from various gold precipitation conditions and hydrothermal fluids compositions. The compositional data obtained from gold samples in this study is considered to provide useful insights from the natural variability of orogenic gold deposits, which can be used to compare with gold composition from other deposit types. However, a larger population of gold grains from a large range of different settings will be needed to completely characterize the composition of gold from orogenic deposits. The key characteristics and geological setting of the selected deposits are presented in Table 1.

2.2. Analytical methods

2.2.1. Electron probe micro-analysis

A total of 224 gold analyses for major (Au, Ag) and minor elements (Zn, Cu, Ni, Co, Fe, Rh, Pb, S, Hg, Pt, Se, As) were obtained with a CAMECA SX-100 electron probe micro-analyzer (EPMA) at Université Laval (Québec, Canada). The device is equipped with 5 wavelength dispersive spectrometers. The analyses were performed using a 25 kV accelerating voltage with 100nA beam current for minor elements and 20nA for major elements, both with a 5 μm beam size. Standard materials were oxides and pure metals from the Astimex company. For each gold grain, we analyzed at least two spots in different positions to check within-grain homogeneity. The average detection limits for each element are: ~2227 ppm for Au, ~1040 ppm for Ag, ~22 ppm for Zn, ~18 ppm for Cu, ~15 ppm for Co, ~22 ppm for Fe, ~21 ppm for Ni, ~56 ppm for Rh, ~85 ppm for Pb, ~128 ppm for Pd, ~28 ppm for S, ~122 ppm for Hg, ~87 ppm for Pt, ~44 ppm for Se, and ~ 47 ppm for As.

2.2.2. Laser ablation-inductively coupled plasma-mass spectrometry

A total of 190 gold analyses by laser ablation-inductively coupled plasma-mass spectrometry (LA-ICP-MS) were carried out at the Geological Survey of Canada (GSC, Ottawa, Canada) and University of New Brunswick (UNB) following the methodology of Milidragovic et al. (2016). At the GSC, gold samples were analyzed using an Agilent Technologies 7700x Series quadrupole ICP-MS coupled to a Photon Machines Analyte 193 nm excimer laser ablation system. The samples were ablated for 60 s in spot mode with a 15 to 40 μm spot size, energy density of ca. 4.2 J/cm^2, and a laser repetition rate of 10 Hz. Trace element contents of Mg, Al, Si, S, Cr, Mn, Fe, Co, Ni, Ti, Cu, Zn, As, Se, Mo, Pd, Cd, In, Sn, Sb, Te, Re, Pt, Tl, Pb, and Bi, were measured. The basaltic glass standard GSE-1G was used for calibration for Mg, Al, Si, Ti, Mo, and Tl employing the GeoReM preferred values from the GeoReM on-line reference materials data base (Jochum et al., 2005). The synthetic pyrrhotite standard Po726 was used for calibration of S, Fe, and PGE (Sylvester et al., 2005). The USGS synthetic MASS-1, a pressed powder pellet, was used for calibration of Hg (Wilson et al., 2002). The synthetic gold standard (NA-Au-31) was used for calibration of other trace element contents in gold (As, Bi, Cd, Co, Cr, Cu, Mn, Ni, Pb, Sn, Sb, Te, Se, Zn) and the gold standards (NA-Au-30 and Au-RM-2) were used for quality control of the LA-ICP-MS analyses (Milidragovic et al., 2016).

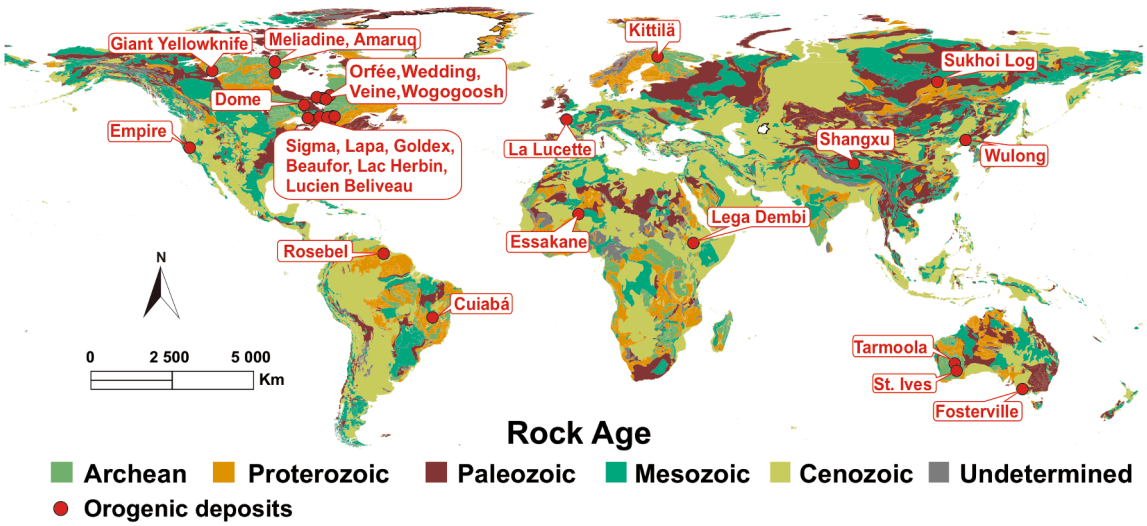

Fig. 1. Distribution of the selected twenty-seven orogenic gold deposits in this study.

Data were reduced using CONVERT and LAMTRACE spreadsheet programs (Jackson & Sylvester, 2008), which employ procedures described by Longerich et al. (1996).

At the UNB, a Resonetics S-155-LR 193 nm Excimer laser ablation system coupled with an Agilent 7700x quadrupole ICP-MS was used to determine the trace element contents in gold. Native gold grains were ablated for 40 s in spot mode with a 24 to 45 μm spot size depending on the gold size, and 30 s for background measurement, energy density of ca. 2.3 J/cm^2, and the beam operating at 3.5 Hz for spot analyses. Acquisition time for all masses was set to ensure higher counting times on more important elements, with a total sweep time of ~ 0.8 s. The same trace element suites as at the GSC are measured at the UNB. The external standard NIST610 was used for calibration of Mg, Al, Si, S, Ti, Mo, In, and Tl (Rocholl et al., 1997). The USGS synthetic standard MASS-1 was used for calibration of Hg (Wilson et al., 2002). The synthetic gold standard (NA-Au-31) was used for calibration of Cr, Mn, Fe, Co, Ni, Cu, Zn, As, Se, Pd, Cd, Sn, Sb, Te, Pt, Pb, and Bi, whereas the gold standard (NA-Au-30) was used for quality control of LA-ICP-MS analyses (Milidragovic et al., 2016). The standards were analyzed every eight samples as same ablation spot size with the sample analysis. Data were reduced using Iolite3.0 software based on standard methods (Longerich et al., 1996; Paton et al., 2011). At both laboratories, one or two spots were analyzed in one gold grain, but more spots were analyzed to check the homogeneity of trace elements in larger gold grains (>100 μm). For internal standardization in both laboratories, element contents were normalized to Ag values determined by EPMA at Université Laval to correct for differing ablation yields. The ranges of detection limits for analyses conducted in both laboratories are reported in Supplementary data 2.

2.3. Data pre-processing

Geochemical data may contain values below the detection limit, which can bias the estimates of mean and variance when applying multivariate statistical methods. Therefore, a replacement value that more accurately reflects an estimate of the true mean and does not affect the covariance of the data set, is required to generate data sets for multivariate analysis. Replacement methods for censored geochemical data and the validation for these methods have been reported in several studies (Grunsky, 2010; Hron et al., 2010; Palarea-Albaladejo et al., 2014; Grunsky and de Caritat, 2020). Element with less than 60% censored data, including Ag (0%) and Fe (25%) contents determined by EPMA, and Cu (0%), Hg (15%), Pd (41%), Pb (54%), and Bi (51%) contents determined by LA-ICP-MS, were investigated by PLS-DA in this study.

In this study, we used the robust multiplicative lognormal replacement method, zCompositions, implemented in the R environment to impute censored data (Palarea-Albaladejo and Martín-Fernández, 2015). Censored geological data were imputed via Expectation Maximization (lrEM function, Palarea-Albaladejo et al., 2007), which converts compositional data into the Aitchison space using the additive log-ratio (alr). The lrEM imputation uses maximum-likelihood estimation and proceeds by replacing values that are missing or below detection limit (BDL, Palarea-Albaladejo and Martín-Fernández, 2015). The imputation of BDL values is not restricted to one limit of detection (LOD), but combines all the aspects of LOD values for the reference such as scale invariance and sub-compositional coherence (Palarea-Albaladejo and Martín-Fernández, 2015). Thus, lrEM can impute the BDL values with a replacement that is between 0 and LOD, which preserves the relative variance structure of the whole censored dataset. The lrEM imputation method has been applied to compute BDL values when applying multivariate statistical methods to explore mineral geochemistry compositions (Cracknell et al., 2019; Grunsky and Caritat, 2017; Dmitrijeva et al., 2019).

Composition data are measured proportions that sum up to a constant value of 1, also called closed data sets (Aitchison, 1986; Aitchison and Greenacre, 2002). Closed geological data can lead to a spurious correlation when studying the relationship within a dataset (Aitchison, 1986). We used the centered log-ratio (clr) transformation, which is recommended for multivariate statistical methods (Makvandi et al., 2016; Grunsky and de Caritat, 2020).

2.4. Partial least squares discriminant analysis

Gold compositional data consist of various elemental variables, forming a high dimensional data set, where a dimension reduction statistical method is preferred to visualize compositional data and to investigate the controls of different geological phenomenon on the gold composition. Partial least squares discriminant analysis (PLS-DA) is a linear classification method, which searches for latent variables with a maximum covariance with the Y-variables (Barker and Rayens, 2003; Brereton and Lloyd, 2014). The main advantage of PLS-DA is that it enhances the separation between groups of observations and identifies variables responsible for the separation of the labeled subgroups. The application of PLS-DA in mineral compositional investigations has been reported in several studies (Makvandi et al., 2016; Huang et al., 2019a, 2019b; Sciuba et al., 2020a, 2020b). In the PLS-DA model, the weights and loadings biplot ($\mathbf{qw}^*_1$-$\mathbf{qw}^*_2$) is used to illustrate the correlations

Table 1
Sample descriptions and geologic background of twenty-seven studied orogenic gold deposits from the Archean to the Cretaceous.

Deposit name	Orogen/craton	Gold occurrence	Host rocks	Metamorphic grade	Mineralization period	Reference
Canada						
Veine	Superior	Anhedral inclusions in quartz or veinlets filling in the fractures of pyrite	Granodiorite	Greenschist	Archean	Hanes et al., 2017; Mercier-Langevin et al., 2012
Wedding	Superior	Anhedral inclusions in pyrite and contact with chalcopyrite	Granodiorite	Greenschist	Archean	
Wogogoosh	Superior	Anhedral inclusions in quartz ± pyrite	Granodiorite	Greenschist	Archean	
Orfée	Superior	Disseminated inclusions in quartz; fine round grain	Mafic rocks	Greenschist	Archean	Bogatu, 2017
Lucien Béliveau	Superior	Anhedral inclusions in pyrite or veinlets filling in fractures in tourmaline; isolated fine grain	Granodiorite	Greenschist	Archean	Pilote, 2000; Daigneault et al., 2002
Sigma	Superior	Anhedral inclusions in quartz or veinlets filling in the fractures of tourmaline; irregular fine grain	Granodiorite	Greenschist	Archean	
Beaufor	Superior	Anhedral inclusions or veinlets in pyrite ± quartz	Granodiorite	Greenschist	Archean	Roussy, 2004
Lapa	Superior	Irregular inclusions in quartz ± chalcopyrite	Granodiorite	Greenschist	Archean	Simard et al., 2013
Lac Herbin	Superior	Irregular inclusions or elongated veinlets in pyrite	Granodiorite	Greenschist	Archean	Rezeau et al., 2017
Goldex	Superior	Anhedral inclusions in pyrite ± quartz or elongated veinlets filling in the fractures of pyrite	Granodiorite	Greenschist	Archean	Dubé and Gosselin, 2007
Dome	Superior	Irregular inclusions in pyrite ± quartz	Mafic rocks	Greenschist	Archean	Robert et al., 1997; Poulsen, 2000
Giant Yellowknife	Slave	Anhedral inclusions in quartz; fine round grain	Basalt	Amphibolite	Archean	Michibayashi, 1995; Shelton et al., 2004
Amaruq	Rae	Anhedral inclusions in arsenopyrite or veinlets filling in fractures in quartz ± tourmaline; isolated fine grain	Mafic rocks	Greenschist	Archean	Côté-Mantha et al., 2017; Valette et al., 2018; Bronac and de Vazelhes, 2019
Meliadine	Rae	Subhedral to anhedral inclusions in pyrrhotite	Gabbro dykes and sills	Lower to middle greenschist	Proterozoic	Carpenter et al., 2005; Lawley et al., 2015
Brazil						
Cuiabá	Sao Francisco	Subhedral to anhedral inclusions in pyrrhotite; fine round to angular grain	Mafic volcanic rocks	Greenschist	Archean	Ribeiro-Rodrigues et al., 2007
Australia						
Tarmoola	Yilgarn	Subhedral to anhedral inclusions in quartz ± arsenopyrite; fine angular to irregular grain	Komatiite, trondhjemite	Greenschist	Archean	Cox and Ruming, 2004; Duuring et al., 2004
St Ives Goldfield	Yilgarn	Anhedral inclusions in pyrite; fine round grain	Dolerite	Upper greenschist	Archean	
Fosterville	Lachlan Fold belt	Subhedral inclusions in quartz; coarse grain	Turbidites	Prehnite-lower greenschist	Ordovician	Mernagh, 2001
Suriname						
Rosebel	Trans-Amazonian Orogen	Anhedral inclusions in tourmaline; fine isolated grain	Felsic to mafic volcanic rocks	Greenschist	Proterozoic	Daoust et al., 2011
Burkina faso						
Essakane	Oudalan-Gorouol belt	Elongated veinlets in fractures in quartz	Turbidites (arenite-argillite)	Lower greenschist	Proterozoic	Tshibubudze and Hein, 2016
Finland						
Kittilä	Fennoscandian (or Baltic) Shield	Anhedral inclusions in arsenopyrite; coarse to fine grain	Mafic rocks and felsic volcanic rocks	Greenschist to granulite	Proterozoic	Eilu et al., 2003; Wyche et al., 2015
Ethiopia						
Lega Dembi	Arabian-Nubian Shield	Subhedral to anhedral inclusions in pyrite ± chalcopyrite; coarse to fine irregular grain	Contact gneiss-volcano-sedimentary	Upper greenschist to lower amphibolite	Cambrian	Billay et al., 1997
Russia						
Sukhoi Log	Siberian	Anhedral inclusions in pyrite; fine irregular grain	Shale, mudstone-sandstone	Greenschist	Carboniferous	Laverov et al., 2000; Large et al., 2007; Meffre et al., 2008
France						
La Lucette	Central-Armorican	Subhedral to anhedral inclusions in quartz ± stibnite; coarse irregular to elongated grain	Black shales	Greenschist	Triassic	Pochon et al., 2016, 2015
USA						
Empire	Cordilleran Orogen	Anhedral inclusions in pyrite ± galena; fine irregular grain	Metavolcanics, serpentinites, granodiorite	Greenschist	Jurassic	Taylor, 2007; Alpers et al., 2014
China						
Wulong	North China Craton	Anhedral inclusions in pyrite ± telluride	Biotite granite	Granulite	Cretaceous	Junhao et al., 2004
Shangxu	Bangong Nujiang suture belt	Irregular inclusions in pyrite ± quartz	Turbidite	Greenschist	Cretaceous	Fang et al., 2020

between elemental variables and relationships between variables and classification groups. Samples grouped in the same quadrant and/or in the vicinity of each other are positively correlated, whereas they are negatively correlated with the variables positioned in the opposed quadrants. The correlation among variables and sample classes control the distribution of samples in the score scatter plot ($\mathbf{t_1}$-$\mathbf{t_2}$). The origin of score scatter plots represents the mean composition of the whole dataset (Makvandi et al., 2016). Elemental variables located at the extreme corners of the weights and loadings plot ($\mathbf{qw^*_1}$-$\mathbf{qw^*_2}$) contribute most to the separation of groups in the scores plot ($\mathbf{t_1}$-$\mathbf{t_2}$), whereas those located near the origin plot have negligible impact on classification in this model. The Variable Importance on Projection (VIP) is used to illustrate the importance of variables in the class discrimination in the scores plot (Eriksson et al., 2001, 2013). Variables with VIP values>1 have more impacts in the model. Variables with a VIP between 0.8 and 1 are moderately influential variables, whereas the VIP with less than 0.8 have smaller contributions to the classification (Makvandi et al., 2016).

3. Results

3.1. Gold texture

The 287 native gold grains studied from orogenic gold deposits are fine- to coarse-grained (5–495 μm), 80% of which range from 20 to 120 μm (Fig. 2A). Three common gold textures have been identified by optical microscopy and back-scattered electron imaging. The dominant native gold texture is anhedral to subhedral inclusions in pyrite (51%), arsenopyrite (36%), chalcopyrite (28%), and pyrrhotite (11%) (Fig. 2B). Selected native gold grains with typical textures from various orogenic gold deposits are shown in Fig. 3. Gold is intergrown with stibnite and arsenopyrite in the La Lucette deposit. Gold from Lapa shows a rim of aurostibite ($AuSb_2$) with arsenopyrite inclusions in the aggregate (Fig. 3O). The second more common gold texture is veinlets filling in fractures in pyrite (30%), quartz (44%), calcite (7%) and tourmaline (13%). Gold from Essakane can occur as single subangular coarse grains intergrown with tourmaline (Fig. 3H), whereas gold is finely disseminated in quartz veins at Orfée. Subhedral gold from Lucien Béliveau is intergrown with Ag-rich telluride (Fig. 3P). These gold grains form veinlets filling in fractures in brittle minerals or between the gap of minerals (Fig. 3D, E, F, G, and 2D). The less common, third gold texture is subhedral isolated grains in quartz veins or rounded grains along the boundaries of sulfides (Fig. 3I, J). The majority of gold grains in this study exhibit a homogeneous elemental distribution and generally contain a low abundance of inclusions of pyrite, arsenopyrite, stibnite, and chalcopyrite under BSE (Fig. 3I, L, and M). However, we cannot exclude the occurrence of micro inclusions within gold grains.

3.2. Geochemistry of native gold

Major and minor element contents in native gold, determined by EPMA, are reported in Supplementary data 1. The Au contents in gold grains show a range from 64 to 99 wt% and Ag contents ranging from 0.6 to 29.8 wt%, respectively. Gold fineness, expressed as $\{Au_{wt.}\%/(Au_{wt.}\% + Ag_{wt.}\%) \times 1000\}$, ranges from 702 to 994, with an average value of 903. Copper, Fe, S, and Hg commonly have concentrations above the detection limit of the EPMA method. However, other minor elements (Zn, Ni, Rh, Pb, Se) have less frequently detected values and thus are not discussed further. Copper content in gold grains from orogenic deposits has a range from 0.0023 to 0.2 wt%. Iron ranges from 0.0022 to 1.1 wt %. Sulfur has a range from 0.0048 to 0.7 wt%. Mercury has an average value of 0.2 wt%, excluding gold grains from Kittilä with an average of 4.5 wt% Hg.

Bivariate plots show that element atomic proportions do not correlate with Au contents for most orogenic gold grains, with the exception of a strong negative linear correlation between Au and Ag (R = 0.98; Fig. 4A). It is notable that there is a broad correlation between Cu content with increasing Au content up to 90 at.%, whereas there is an inverse trend between Cu and Ag contents. Above 90 at.% Au, the Cu content shows a broad decrease with increasing gold (Fig. 4B). For some gold deposits, there are correlations between Au and Fe, and Hg. For instance, at Tarmoola, there is a moderate negative linear correlation between Au and Fe (R = 0.70) and a weak positive correlation between Ag and Fe (R = 0.45) (Fig. 4E and H). A strong negative linear correlation is observed between Au and Fe (R = 0.96) at Goldex (Fig. 4E). There is a strong negative correlation between Au and Hg (R = 0.90) and a weak positive correlation between Ag and Hg (R = 0.34) in gold from Kittilä (Fig. 4C and I). For gold from other orogenic gold deposits, there are not significant correlations between Au and Fe, Hg, S, and As.

Trace element contents in native gold determined by LA-ICP-MS are reported in Supplementary data 3. The ranges in contents of twenty-four trace elements from 190 gold analyses are displayed in a multi-element box-whisker plot (Fig. 5). As the lithophile (Mg, Al, Ca, and Si) elements likely are from sub microscopic or below surface inclusions of gangue minerals, and do not show discriminant signatures for fingerprinting Abitibi greenstone belt orogenic deposits (Velasquez, 2014), hence, they are not discussed in this study. Fig. 5 indicates that, for the majority of

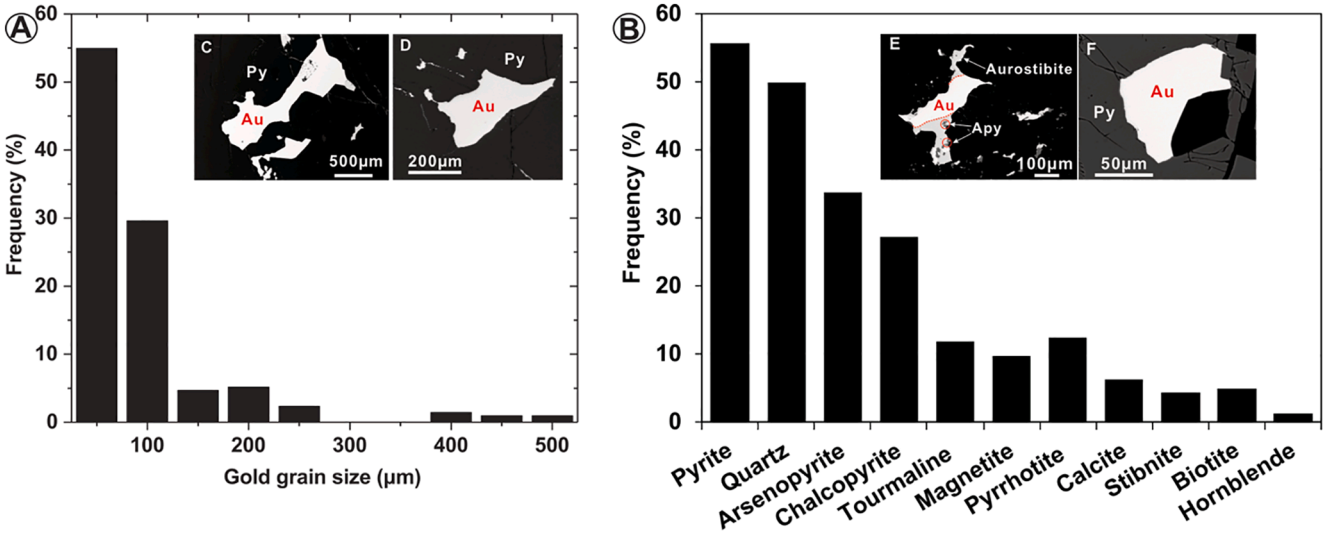

Fig. 2. Histograms of gold grain sizes and mineral associations. (A) Histogram of grain sizes of 287 gold samples. (B) Histogram of mineral association of 287 gold samples.

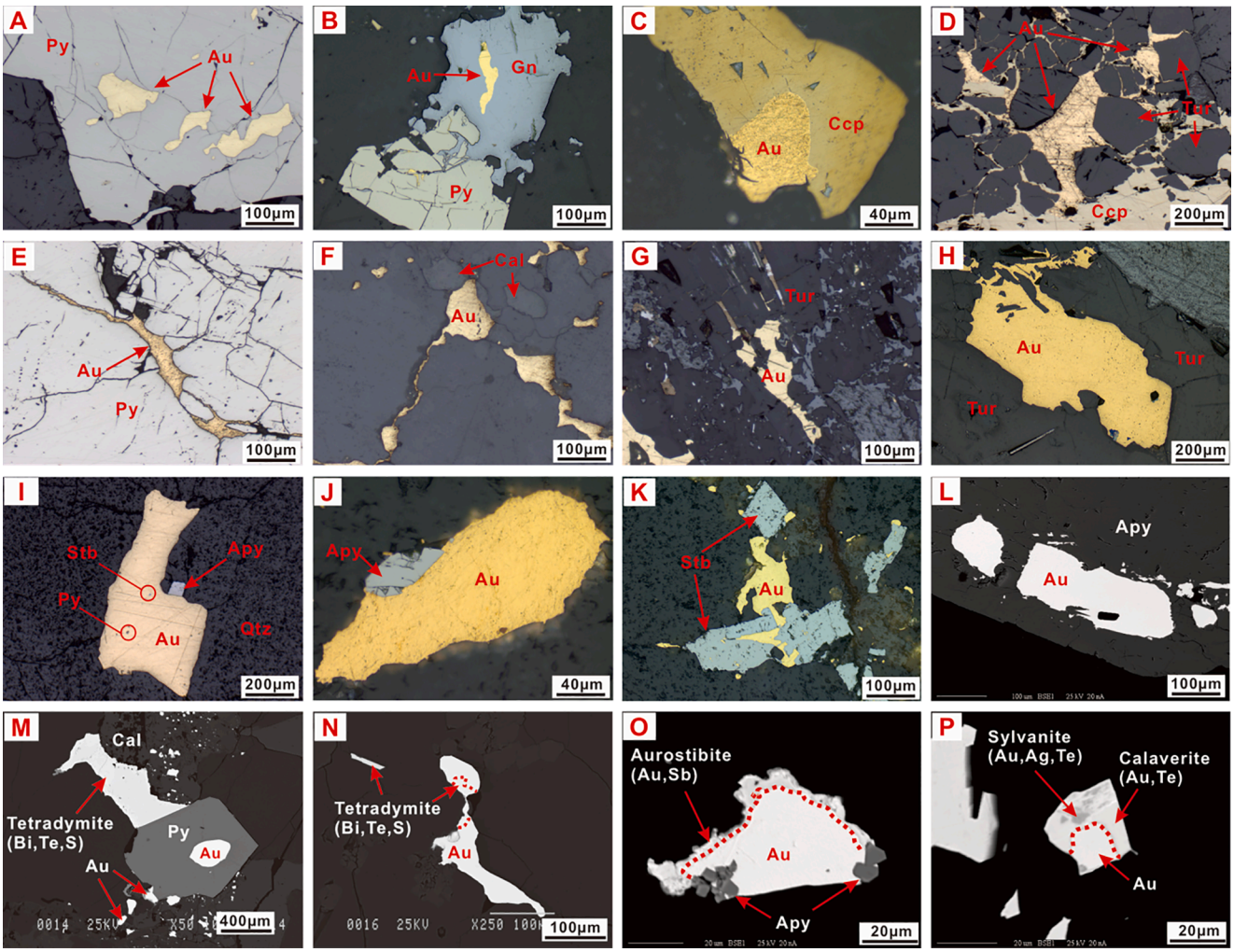

Fig. 3. Selected native gold grains with typical textures from various orogenic gold deposits. (A) Anhedral gold inclusions in pyrite from Lucien Béliveau. (B) Gold elongated inclusions in galena intergrown with euhedral pyrite from Empire. Minor gold is found in fractures in pyrite. (C) Rounded gold inclusion in chalcopyrite from Lega Dembi deposit. (D) Coarse gold in fractures in tourmaline and along the boundary of chalcopyrite from Beaufor deposit. (E) Elongated gold veinlets in fractures in pyrite from Goldex. (F) Anhedral gold veins in association with calcite from Giant. (G) Anhedral gold grains in tourmaline from Sigma. (H) Coarse anhedral gold grain is hosed in tourmaline from Essakane. (I) Coarse gold in contact with arsenopyrite in a quartz vein. Small stibnite and pyrite inclusions in gold from Fosterville. (J) Isolated gold is contact with arsenopyrite from Lapa. (K) Anhedral gold intergrown with euhedral stibnite in quartz veins from La Lucette. (L) Back-scattered electron image of subrounded gold inclusions in arsenopyrite from Kittilä. (M) Rounded gold inclusion in euhedral pyrite in contact with telluride in a calcite vein from Beaufor. (N) Elongated gold in a vein in association with tellurides from Beaufor. (O) Back-scattered electron image of gold with a rim of aurostibite in association with arsenopyrite from Lapa. (P) Anhedral gold coated by Ag-rich telluride film from Lucien Béliveau. Abbreviations: Au-gold; Py-pyrite; Apy-arsenopyrite; Ccp-chalcopyrite; Cal-calcite; Stb-stibnite; Qtz-quartz; Tur-tourmaline; Gn-galena.

the elements, there is at least one order of magnitude variability of the contents at the 25th to 75th percentile range. The comparison of element content from EPMA and LA-ICP-MS for Cu, Hg, and Fe shows similar average, median, and range of concentrations for both analytical methods with lower concentrations detected by LA-ICP-MS (Fig. 6). The main difference is S data where EPMA analyses yield an order of magnitude greater mean value than the LA-ICP-MS data, and this is likely due to large variations of detection limits of LA-ICP-MS. The higher detection limit by LA-ICP-MS is related to smaller laser beam sizes. Alternatively, due to the higher volatility of S, significant fractionation of S relative to Fe (and Co, Ni, Cu) may occur during LA-ICP-MS analyses (Gilbert et al., 2014). Therefore, the S contents determined by LA-ICP-MS are not taken into consideration in PLS-DA analysis.

3.3. Multivariate statistics of gold trace element composition

The data set reported in this study are not large enough for deposit scale studies, but we can group gold compositional data in relation to petrographic observations (Fig. 3) and documented geological information in literature (Table 1). Thus, geological factors, including mineral association, occurrence texture, and dominant country rock composition, are investigated by PLS-DA to identify controls on the trace element composition in gold grains from studied orogenic deposits.

3.3.1. Gold composition in relation with mineral association

For the purpose of PLS-DA, the mineral association with gold paragenesis is hereby simplified to record the host mineral of an inclusion or the co-existing minerals. Based on petrography, mineral associations are simplified into the arsenopyrite-pyrite-magnetite-stibnite (Apy-Py-Mag-Stib), pyrite-arsenopyrite-pyrrhotite-galena-chalcopyrite (Py-Apy-Po-Gn-Ccp), and tourmaline-quartz-calcite (Tur-Qtz-Cal) assemblages. The loadings biplot of the first and second PLS-DA components (**qw*$_1$-qw*$_2$**, Fig. 7A) illustrates positive correlations between Bi, Sb, and Ag within negative first (**qw*$_1$**) and positive second components (**qw*$_2$**), whereas Fe and Cu with positive **qw*$_1$** and negative **qw*$_2$**, have negative correlations with Bi, Sb, Ag. There are positive correlations between Pb and

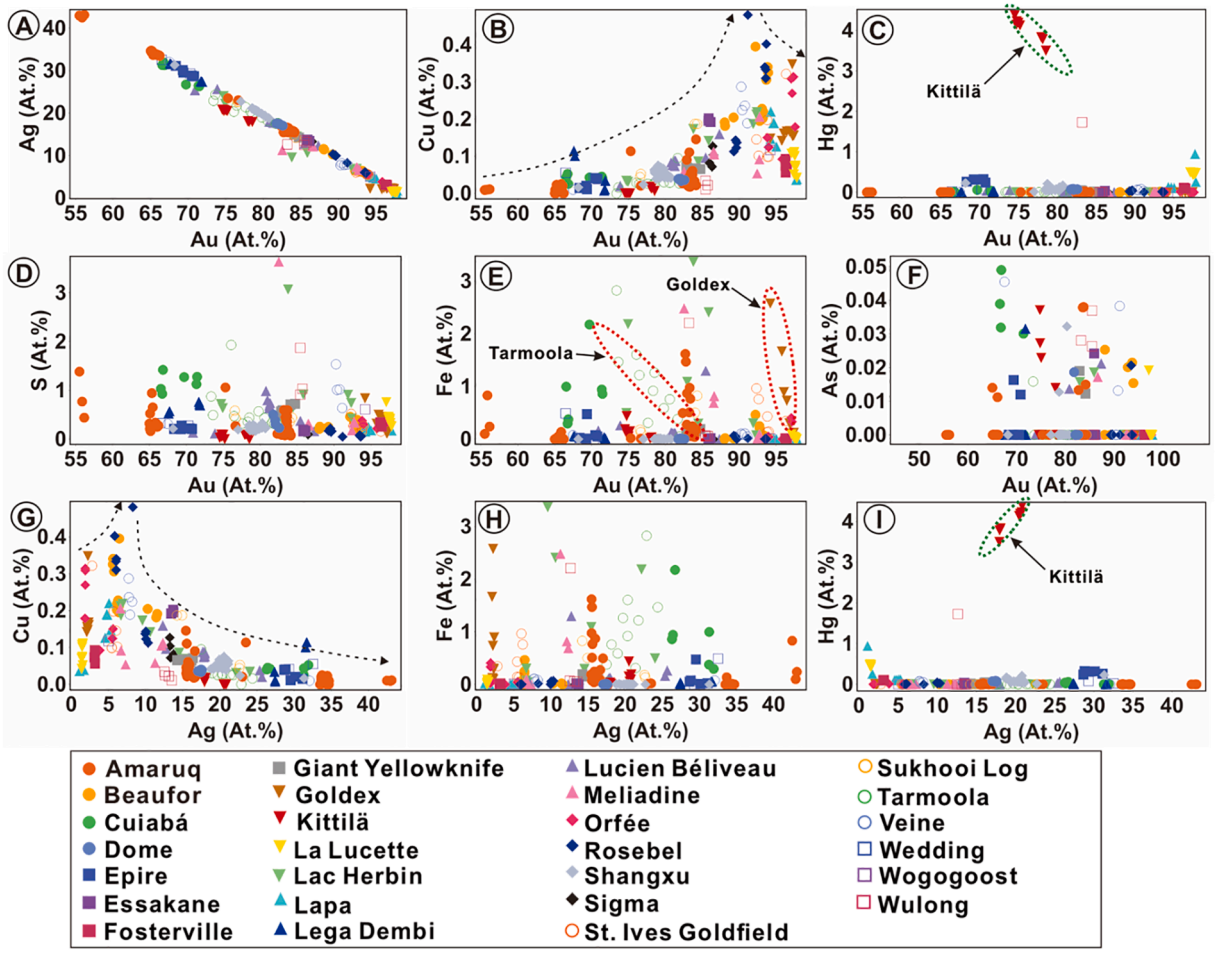

Fig. 4. Bivariate EPMA plots showing major and minor element atomic percentages (at.%) and trends in native gold. (A) Au versus Ag, (B) Au versus Cu, (C) Au versus Hg, (D) Au versus S, (E) Au versus Fe, (F) Au versus As, (G) Ag versus Cu, (H) Ag versus Fe, (I) Ag versus Hg. The red dashed circles indicate negative correlations between Au and Fe from Tarmoola and Goldex deposits. The green dashed circles indicate correlations between Au and Hg, Ag and Hg, from Kittilä deposit.

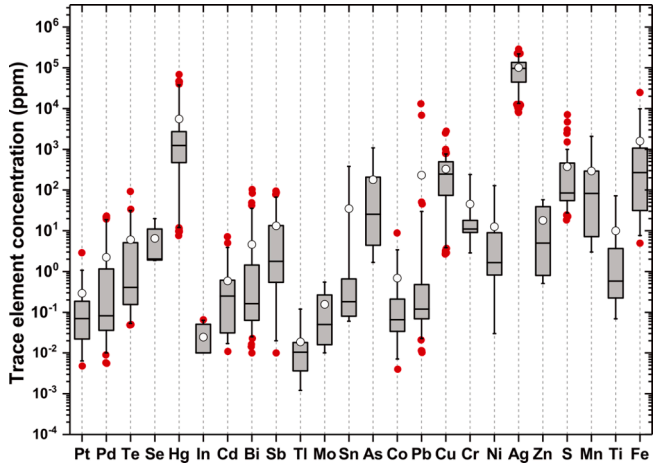

Fig. 5. Multi-element box (25th – 75th percentile) and whisker (5th – 95th percentile) plots for LA-ICP-MS trace element concentration of 190 native gold analyses from twenty-seven orogenic gold deposits. The red circles indicate the outlier valued beyond the range of 5th – 95th percentile. Short line within the box represents the median value, whereas the white circle on the whisker indicates the mean value. All the trace element concentrations determined by LA-ICP-MS are filtered by the limit of detection (LOD) for each analysis.

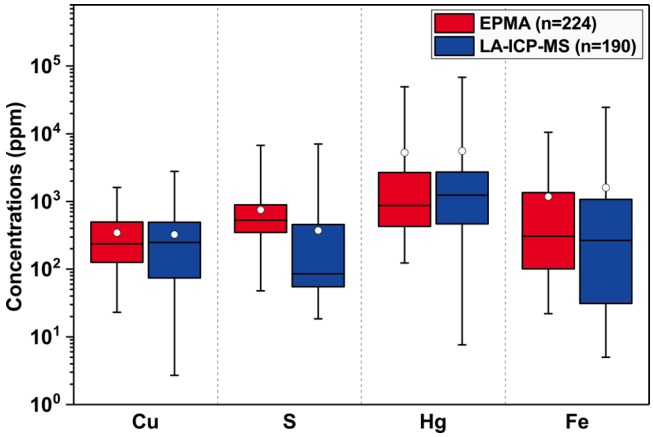

Fig. 6. Comparison of the element concentration in gold grains determined by EPMA and LA-ICP-MS. The whisker plots indicate the range between minimum and maximum values. Short line within the box represents the median value, whereas the white circle on the whisker indicates the mean value.

Pd with negative **qw*$_1$** and **qw*$_2$** values, whereas Pb and Pd have negative correlations with Hg, which have positive **qw*$_1$** and **qw*$_2$** values. The distribution of samples on the scores plot (**t1-t2**) shows that the three groups form overlapping clusters due to the simplification of

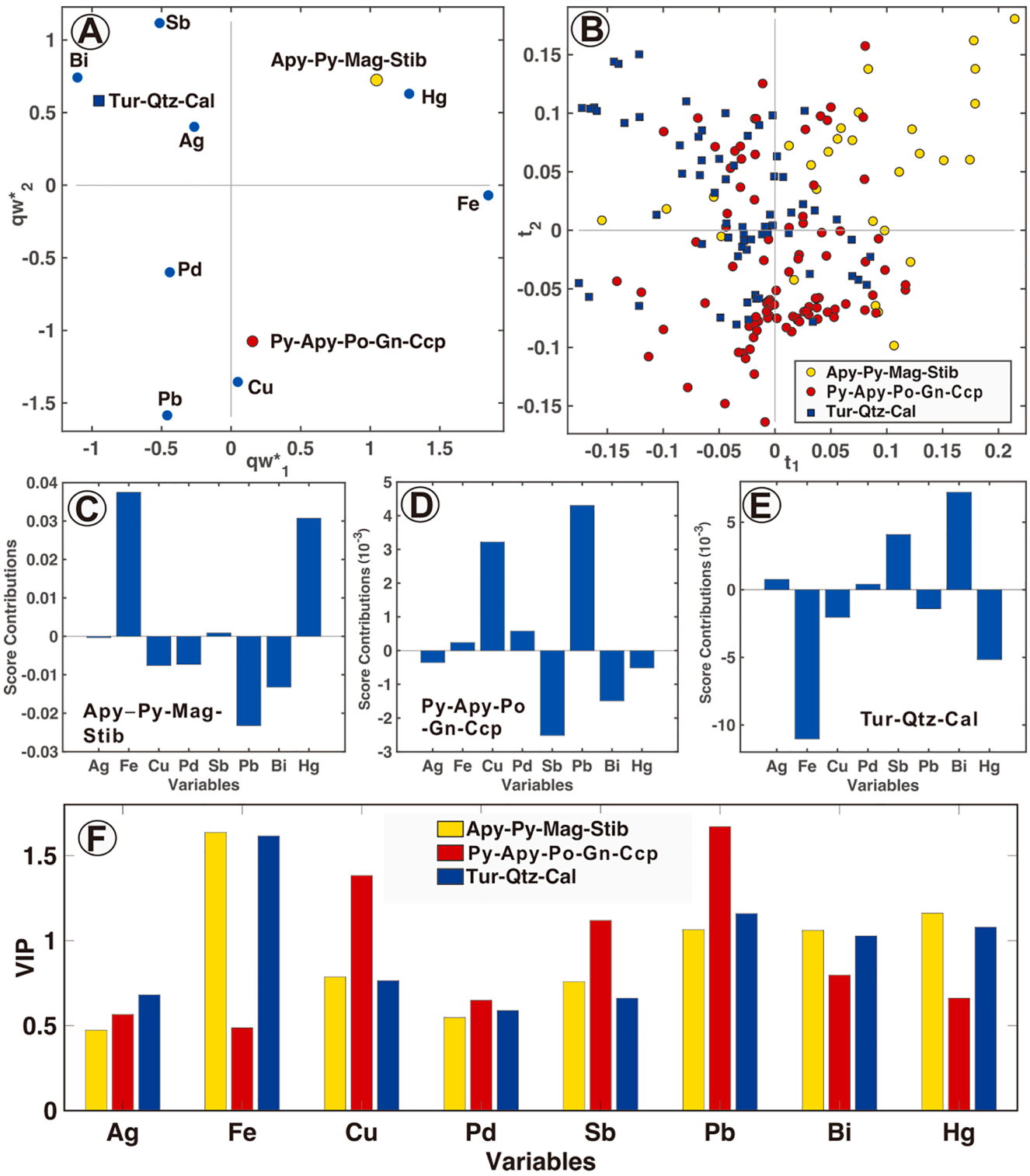

Fig. 7. The PLS-DA plot of LA-ICP-MS compositional data for native gold from different mineral associations in studied orogenic gold deposits. (A) The first and second loadings plot (**qw*$_1$-qw*$_2$**) indicate correlations among elemental variables and mineral association. (B) The first and second scores plot (**t1-t2**) shows the distribution of gold analyses classified by mineral associations from various orogenic gold deposits in the latent variable space defined by loadings (**qw*$_1$-qw*$_2$**). (C) Score contributions of Apy-Py-Mag-Stib assemblages. (D) Score contributions of Py-Apy-Tur-Po-Gn-Ccp assemblage. (E) Score contributions of Tur-Qtz-Cal assemblage. (F) The variable importance on the projection (VIP) values reflect the significance of compositional variables for classification of samples in the score plot (**t1-t2**). Py-pyrite; Apy-arsenopyrite; Mag-magnetite; Ccp-chalcopyrite; Stib-stibnite; Gn-galena; Po-pyrrhotite; Tur-tourmaline; Qtz-quartz; Cal-calcite.

the complex mineral combinations with quartz-calcite (Fig. 7B), though they can be distinguished through their distinct mean compositions from variable score contribution plots (Fig. 7C-E). For instance, gold intergrown with the Apy-Py-Mag-Stib assemblage can be discriminated mainly because of high Fe and Hg, lower Pb and Bi relative to the average of the whole dataset (Fig. 7C). In contrast, higher Cu and Pb and lower Sb discriminate the gold associated with the Py-Apy-Po-Gn-Ccp assemblage (Fig. 7D), whereas the Tur-Qtz-Cal assemblage forms a

cluster with positive **t1** and **t2** values because of relatively high Sb, Bi, and low Fe, Cu, Pb, Hg. The VIP plot also shows that Pb is an important element in classification of all three groups (VIP > 1), whereas the contribution of Ag and Pd to the classification is negligible (VIP < 0.8). Additionally, Cu and Sb are important in the classification of Py-Apy-Po-Gn-Ccp assemblage, whereas Fe, Bi and Hg are important for the separation of the other two groups (Fig. 7F).

3.3.2. Gold composition in relation to texture

Native gold is divided into two common textures, gold inclusions and gold filling fractures. The first and third principle components plots (**qw*$_1$-qw*$_3$**) show the better classification relative to the combination of first and second components in discriminating the two textures. The loadings plot (**qw*$_1$-qw*$_3$**) indicates there are strong positive correlations between Fe, Pb, Cu, Pd, and between Sb, Bi, which consequently contribute to the sample distributed in Fig. 8B. Palladium, Cu, and Hg also indicate their negligible contributions on the classification as they plot close to the center of the loadings plot (Fig. 8A). Even though there is large overlapping between the two groups, as scores contribution plots in Fig. 8C and D depict, they are characterized by distinct variations in Ag, Fe, and Bi compared to mean compositions of the whole dataset. The majority of gold inclusions plot with negative **t1**, because of relatively high Ag, Fe, and Pb (Fig. 8B and D).

3.3.3. Gold composition in relation to country rock composition

The country rock compositions are summarized from descriptions of the selected orogenic gold deposits and labelled according to the dominant lithologic assemblage (Table 1). The first and second loadings plot (**qw*$_1$-qw*$_2$**) in Fig. 9A shows a positive correlation between Ag and Pb both with negative **qw*$_1$** and positive **qw*$_2$** values, and between Sb and Fe, which lie in the negative **qw*$_1$** and **qw*$_2$** quadrant. There is a negative correlation between Hg, Cu and the group of Sb, Fe plotting in the opposite quadrant (Fig. 9A). Copper shows an inverse relationship with Sb in **qw*$_1$** but with **qw*$_2$** values close to 0, indicating they have negligible contributions on the second component (**qw*$_2$**). This characteristic contributes to distinguishing gold hosted by ultramafic–mafic

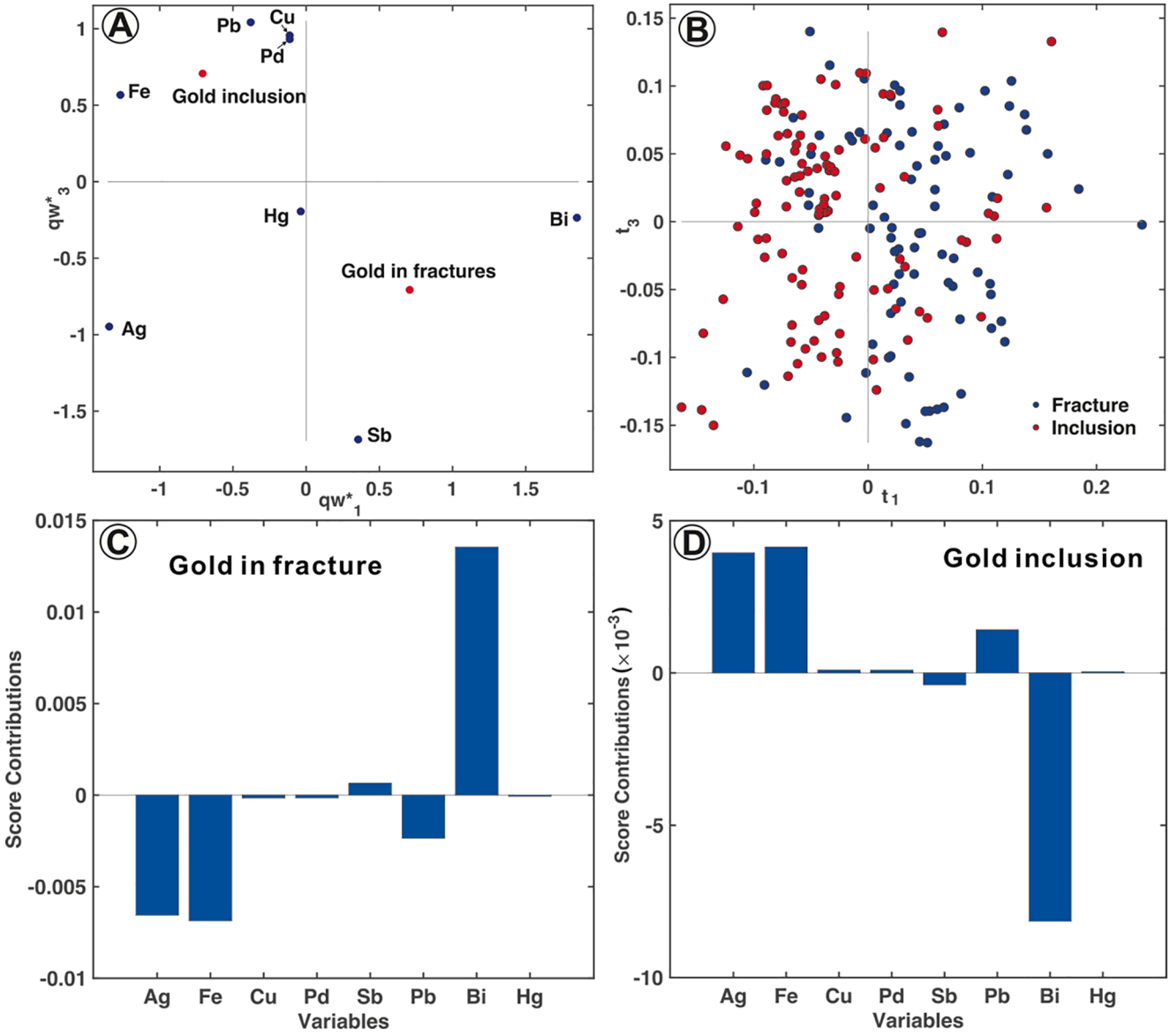

Fig. 8. The PLS-DA plot of LA-ICP-MS compositional data for native gold from different textures of native gold from studied orogenic gold deposits. (A) The first and third loadings plot (**qw*$_1$-qw*$_3$**) indicate correlations among elemental variables and gold textures. (B) The first and third scores plot (**t1-t3**) shows the distribution of gold analyses classified by textures from various orogenic gold deposits in the latent variable space defined by loadings (**qw*$_1$-qw*$_3$**). (C) The score contribution plots of gold veinlets in fractures. (D) The score contribution plots of gold inclusions.

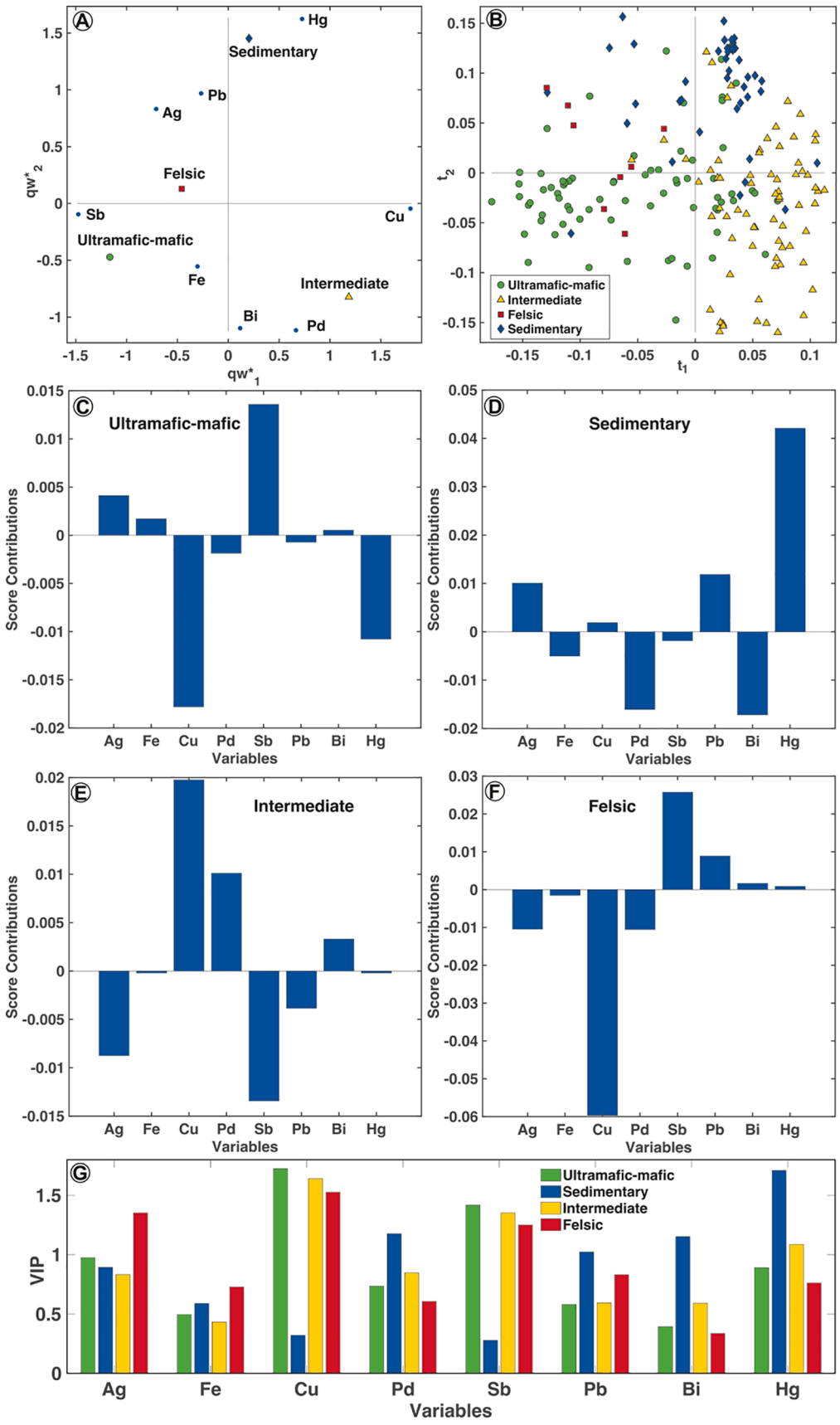

Fig. 9. The PLS-DA plot of LA-ICP-MS compositional data for native gold classified by dominant host rocks of studied orogenic gold deposits. (A) The first and second loadings plot (**qw*$_1$-qw*$_2$**) indicate correlations among elemental variables and dominant host rocks. (B) The first and second scores plot **(t1-t2)** shows the distribution of gold analyses classified by dominant host rocks from various orogenic gold deposits in the latent variable space defined by loadings (**qw*$_1$-qw*$_2$**). (C) Score contribution plot of gold hosted in ultramafic-mafic rocks. (D) Score contribution plot of gold hosted in sedimentary rocks. (E) Score contribution plot of gold hosted in intermediate igneous rocks. (F) Score contribution of gold hosted in felsic igneous rocks. (C) The VIP values reflect the significance of compositional variables corresponding to the classifications of samples in score plot (**t1-t2**).

igneous rocks from intermediate igneous rocks in the scores plot (**t1-t2**). In contrast, Hg and Pb shows an inverse relationship with Bi and Pd along the second component (**qw*$_2$**), which characterizes the gold hosted in sedimentary rocks by high Hg, Pb and low Bi, Pd (Fig. 9B). Gold hosted by ultramafic–mafic igneous rock clusters mainly in the negative **t1** and **t2** quadrant because of high Sb, and low Cu, Hg, whereas gold hosted by intermediate igneous rocks clusters mainly at positive **t1** and negative **t2**, characterized by high Cu, Pd, and Bi (Fig. 9B). There is overlap between gold hosted by ultramafic-mafic igneous rocks and felsic igneous rocks, because gold hosted by felsic igneous rocks is not well discriminated by low negative **qw*$_1$** and positive **qw*$_2$** close to 0, in contrast, gold hosted in ultramafic-mafic rocks cluster in negative **qw*$_1$** and **qw*$_2$** (Fig. 9B). However, gold hosted by felsic rocks is characterized by relatively high Sb, Pb, Bi, Hg, and low Ag, Cu, Pd (Fig. 9F). The VIP plot also shows that Cu, Sb, and Hg, with VIP > 1 are the most important discriminators in classifying gold in relation to different host rock compositions. Trace elements, Fe and Bi with VIP < 0.5, are the least important elements for distinguishing gold hosted in different igneous rocks (Fig. 9G). The variable contributions presented in the Fig. 9C, D, E, and F indicate the mean composition of each host rock subtype is characterized by gold chemical signatures.

4. Discussion

4.1. Inclusions in native gold

There is evidence suggesting that micro-inclusion suites in native gold can provide a characteristic signature for comparing different mineralization types (Potter and Styles, 2003; Chapman et al., 2009, 2010b, 2017, 2018; Dvorani, 2016). In gold grains from orogenic deposits, small sulfide inclusions (2–5 μm) form either irregular blebs or euhedral grains (Fig. 2I). Samples with arsenopyrite inclusions, smaller than the laser ablation spot or which are not exposed on the gold surface, can be recognized from the time-resolved LA-ICP-MS signal spectrum (Fig. 10). In these analyses, signals for inclusion minerals that do not represent the composition of gold were excluded when reducing the LA-ICP-MS data. Inclusions may also consist of a complex association of several phases. For instance, minor stibnite and pyrite form fine-grained inclusions in a coarse gold grain from Fosterville (Fig. 2I). A small proportion of other inclusions, such as arsenopyrite, magnetite, and pyrrhotite, are found in gold from Lapa, Meliadine, and Orfée (Fig. 2O). Chapman and Mortensen (2016) demonstrated that pyrite is the most common inclusion in gold grains from orogenic deposits in the Cariboo Gold District, British Columbia. Overall, compositional data show that most gold grains from the selected orogenic deposits are homogeneous in major element composition under BSE, or that the inclusions are either absent or too small to be detected by SEM. The presence of simple inclusion assemblages (e.g., pyrite, arsenopyrite, pyrrhotite) is in agreement with studies of orogenic gold in British Columbia and Yukon (Chapman et al., 2010a; Chapman and Mortensen, 2016). Even though tiny stibnite form inclusions in gold from the Fosterville and La Lucette deposits (Fig. 3I), Sb does not show significant contributions to distinguish gold with the arsenopyrite-pyrite-magnetite-stibnite assemblage from other mineral association assemblages (Fig. 7C). This indicates that undetected inclusion minerals in gold do not impact significantly the chemical signature of gold in different groups in PLS-DA models. However, the common sulfide inclusion suite (Fe-As-Sb-S) observed in gold from orogenic deposits analyzed in this study, can be used to compare with the inclusion signatures reported from other mineralization types. The inclusion suite coeval with gold is therefore characteristic, as shown by the Pd-Ag-Te-S inclusion suite observed in gold from a skarn mineralization and the Bi-Cu-Te-S-Pb-Sb inclusion suite in gold related to an intrusion-related gold mineralization in the Estero Hondo deposit (Ecuador, Potter and Styles, 2003), whereas the Bi-Pb-Te-S inclusion suite in gold is linked with calc- alkalic porphyries from Yukon (Canada, Chapman et al., 2018).

4.2. Solid solutions in native gold

The strong negative linear correlation, between Au and Ag, with R = 0.98, indicates that silver occurs in solid solution with gold (Fig. 4A). This occurs because of the close similarity in the atomic radius of Au and Ag, such that Ag atoms easily replace Au atoms (Morrison et al., 1991; Hough et al., 2009; Williams-Jones et al., 2009). As previous authors have suggested, lower temperatures correlate with lower Au/Ag ratio in the alloy, whereas a lower pH depresses the Ag content in gold (Morrison et al., 1991; Gammons and Williams-Jones, 1995). The range in fineness, from 702 to 994, is consistent with previous studies that reported the gold fineness from 780 to 1000 in Archean deposits (Morrison et al., 1991; Pal'yanova, 2008). The Cu-rich gold from studied orogenic deposits is likely because of the Au-Ag-Cu complete solid-solution depending on the mineralization temperature (Raynor, 1976;

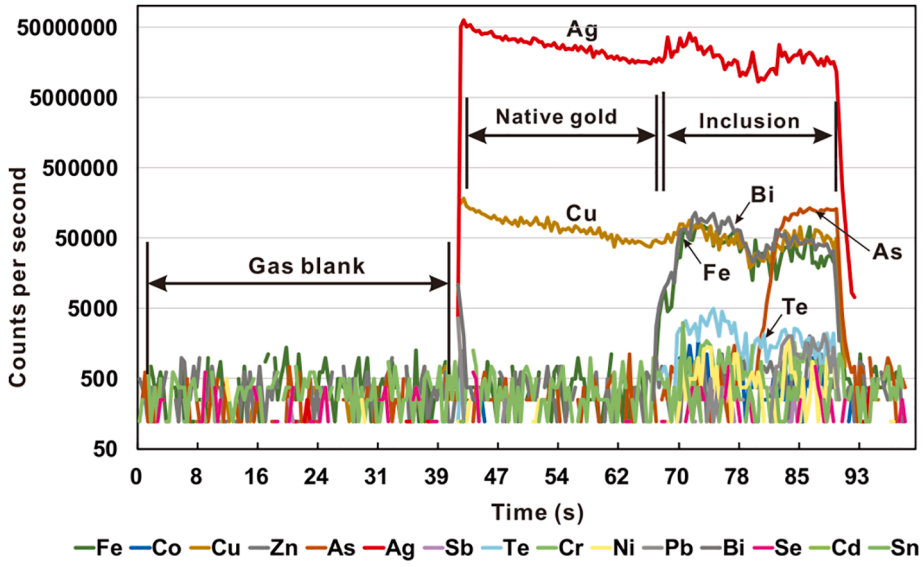

Fig. 10. Representative time-resolved depth profiles for gold grains (samples from Rosebel, Suriname) analyzed in this study indicating the occurrences of inclusions. The spiky Ag indicates the heterogeneous concentration of Ag in the gold. The elevated Fe, Cu, Bi, and Te contents suggest the presence of Fe-Cu-Bi-Te phase micro inclusions under the surface of gold grain, whereas elevated As and Fe indicate that arsenopyrite is likely present in the structure of native gold.

Chudnenko and Palyanova, 2016). Higher Cu values (up to 0.4 at%) correlate with higher fineness but lower Ag among all the gold grains from this study, showing a mutually reverse relationship between Cu-Au vs. Cu-Ag (Fig. 4B and G). This relationship has also been observed in gold grains from the Koyukuk-Chandalar mining district (Alaska, Mosier et al., 1989), the Ballincurry River (Ireland, Moles et al., 2013), the Copper Mountain area (Canada, Chapman et al., 2017), and the Meyos Essabikoula area (Cameroon, Nguimatsia Dongmo et al., 2019). Copper is usually transported as a chloride complex or as a hydrosulfide complex at high concentrations of reduced sulfur and the solubility of Cu is highly depended on temperature (Mountain and Seward, 2003). Chapman et al. (2005) interpreted the elevated Cu in the alloys, and Cu sulfide inclusions in Scottish gold, to indicate a relatively high-sulfidation environment. This scenario is consistent with the findings that gold richer in Cu is correlated with a plutono-volcanic event in the Rosebel gold district (Daoust et al., 2011), and higher temperature fluids at the Beaufor, Goldex, and Lac Herbin deposits (Rezeau et al., 2017; Daver et al., 2020). We propose that the elevated Cu contents in gold grains from some orogenic gold deposits may be suggestive of higher temperature hydrothermal fluids or contributions from a magmatic hydrothermal system.

It is likely that Fe, S, Hg, and As occur in native gold in the form of lattice impurities or sub-micrometer or nanoparticle inclusions, as suggested by the lack of correlation between these elements and Au or Ag (Fig. 4). One possible interpretation is that the differences in ionic radius, between Ag^{1+} (1.26 Å), Au^{1+} (1.37 Å), and Fe^{2+} (0.76 Å), Hg^{1+} (1.19 Å), S^{4+} (0.37 Å), As^{5+} (0.47 Å), creates small interatomic gaps or lattice distortions which allows for the incorporation of other trace element impurities, even though gold is generally considered to be a relatively poor host for trace elements compared with sulfides (Antweiler and Campbell, 1977; Boyle, 1979; Railsback, 2003). Copper is present in gold alloys as a trace element in most studies (Knight et al., 1999; Chapman et al., 2011; Omang et al., 2015; Gas'kov, 2017). Copper is ~ 12% smaller in atomic radius, whereas Cu^{+} is ~ 30% smaller in ionic radius, than Au^{+}, resulting in lattice distortions when Cu replaces Au in the crystal (Hough et al., 2009). Therefore, even small proportions of Cu in gold can lead to lattice distortion in the octahedral site, which would provide space for ion impurities (Chouinard et al., 2005). The negative correlation between Au and Fe at Tarmoola and Goldex indicates that Fe probably replaces Au in solid solution (Fig. 4E). This substitution has also been reported for gold hosted in cosalite at Dublin Gulch, a reduced-intrusion related gold deposit (Cave et al., 2019). However, this is not common in most other orogenic gold deposits, because of the differences in ionic radii and valence between Au^{1+} (1.37 Å) and Fe^{2+} (0.76 Å). There is a slight negative correlation between Sb and Au, indicating the substitution between Au^{3+} and Sb^{3+} due to their similar radius (Fig. 11A). There is no significant correlation between Pb and Au in gold, thus Pb seems not to be solid solution but instead forms impurities in gold (Fig. 11B).

Mercury has been suggested as a useful discriminator for gold from alkalic porphyry and orogenic deposits in British Colombia (Chapman et al., 2017). Gold grains from alkalic porphyry deposits are reported to have higher contents of Hg than gold from the epithermal Black Dome deposit and orogenic deposits in the Cariboo Gold District (Banks et al., 2018). High levels of Hg, however, have been recognized in Au-Ag alloy from some orogenic gold deposits, such as the Violet occurrence, Klondike (Yukon) with 9 wt% Hg (Chapman et al., 2010a). Gold from studied orogenic deposits has relatively low contents of Hg (average at 0.5 wt%), but the Hg content in gold grains varies from site to site (Supplementary data 1). Mercury-rich gold has been reported to be related to low temperature mineralization stages (Gas'kov, 2017). Gold alloys with elevated Hg contents are also reported in porphyry (Sammelin et al., 2011), epithermal (Pearcy and Petersen, 1990), and VMS deposits (Nysten, 1986; Wagner et al., 2007). Several parameters have been proposed to control the concentration of Hg in gold alloys, such as temperature (Rushton et al., 1993), vapor transportation, and fluid composition (Chapman et al., 2010b), however, the mechanisms of transport of Hg, and its partitioning into gold in orogenic systems, are not sufficiently well understood (Chapman et al., 2010b). Mercury is not commonly detected by EPMA in gold from studied orogenic deposits, whilst the highest average value occurs at Kittilä (average 4.45 wt%, Supplementary data 1). However, the negative correlation between Au and Hg in gold from Kittilä suggests that Hg increases at the expense of Au in Au-Ag-Hg alloys (Fig. 4C and I). Due to the mobility of Hg at low temperature, the Hg-rich gold in Kittilä is likely related to retrograde metamorphism, which has been indicated in most of metamorphosed orogenic gold deposits in Finland (Eilu et al., 2003; Wyche et al., 2015).

4.3. Controls of mineral association on gold composition

The presence or absence of co-crystallizing minerals with native gold may influence trace element incorporation into gold. Copper, Pb, and Sb are important discriminators to classify gold associated with the Py-Apy-Po-Gn-Ccp assemblage (Fig. 7F), however, their chemical partitioning preferences seem to be different. Copper and Pb show positive contributions to discriminate gold associated with chalcopyrite and galena, but negative contributions in gold either associated with the arsenopyrite-pyrite-magnetite-stibnite or the tourmaline-quartz-calcite assemblages, which suggests that co-existing chalcopyrite and galena have no significant impacts on the gold composition, likely because Cu- and Pb-rich fluids were not depleted in Cu or Pb by precipitation of sulfides (Fig. 7D).

There is a broad negative covariation of Sb with Au for gold associated with the Py-Apy-Po-Gn-Ccp assemblage, whereas Sb is low in gold associated with Apy-Stib-bearing assemblage (Fig. 11A). One possible explanation is the partitioning of Sb between co-crystallizing stibnite and gold, whereby precipitation of stibnite from sulfur-bearing fluids leads to removal of Sb from the system and forms the Sb-poor native gold. In addition, it has been reported that Sb can substitute for As in the crystallization of arsenopyrite at low temperature, therefore also

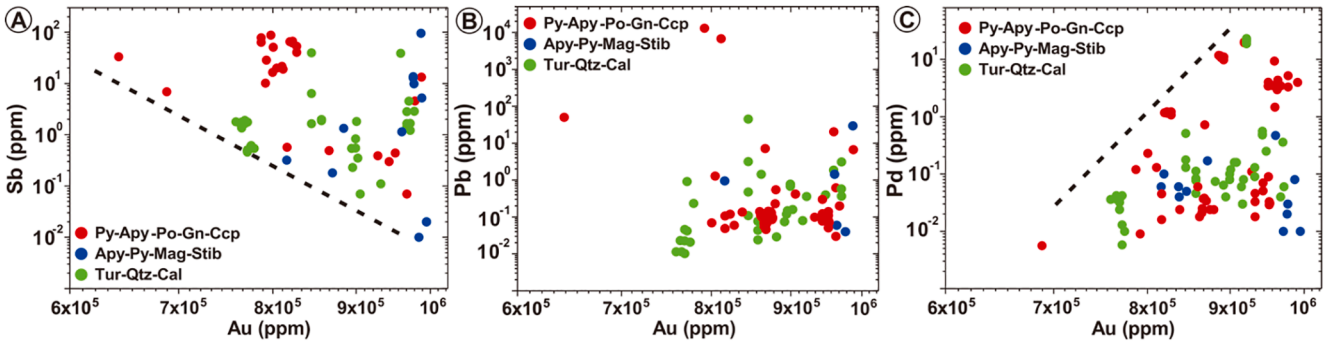

Fig. 11. Bivariate plots showing the correlations between Au and trace elements in native gold. The data comes from Supplementary data 3 and the classifications correspond to PLS-DA in relation to mineral associations. (A) Au versus Sb, (B) Au versus Pd, (C) Au versus Hg, (D) Au versus Pb.

depleting Sb content in the hydrothermal fluid (Fleet and Mumin, 1997; Ashley et al., 2000; Tomkins et al., 2006), such that Sb-bearing arsenopyrite can also lead to Sb-poor gold. Positive contributions of Ag, Bi and Sb discriminate gold associated with the Tur-Qtz-Cal assemblage, indicating that Ag, Bi, and Sb partition into gold where sulfides are absent. However, the concentration of Bi in gold is depressed where chalcopyrite and/or pyrite crystallizes, indicating that Bi is incorporated preferentially into chalcopyrite and/or pyrite in the presence of gold. This is consistent with the findings that chalcopyrite and/or pyrite hosts greater concentrations of Bi in different ore types (George et al., 2018).

Elevated Pd in placer gold likely indicates formation by oxidizing, low temperature chloride hydrothermal systems (Gammons et al., 1993; Chapman et al., 2009). Higher concentration of Pd (>10 ppm) in gold from studied orogenic deposit associated with the pyrite-chalcopyrite assemblage suggests that precipitation of pyrite or chalcopyrite does not depress the Pd concentration in fluids compared to gold associated with other mineral assemblages (Fig. 11C). Therefore, the presence of trace elements in gold may be controlled by the partition preference between gold and co-existing minerals.

4.4. Controls by hydrothermal fluid composition

The two common gold textures in orogenic deposits are gold occurring as inclusions and in veinlets (Fig. 2), with different chemical signatures (Fig. 8). It has been demonstrated that $Au(HS)_2^-$ is the dominant phase to transport Au in near neutral and low salinity orogenic hydrothermal systems at low temperatures (250–350 ℃, Goldfarb et al., 2005; Williams-Jones et al., 2009). Gold is commonly precipitated in an assemblage of pyrite, arsenopyrite, chalcopyrite and pyrrhotite in orogenic deposits, likely because sulfur is consumed to form sulfides when Au-bearing solution reacts with metals with a decrease in oxygen fugacity and the Au-S complex breaks down (Fig. 12; Gammons and Williams-Jones, 1995; Williams-Jones et al., 2009; Garofalo et al., 2014; Goldfarb and Groves, 2015). Gold inclusions in sulfides can be recognized by chemical signatures with positive contribution of Ag, Fe, Pb, and negative contribution of Sb, Bi by PLS-DA (Figs. 8 and 12). In contrast, gold in fractures, likely related to a latter fluid event, is characterized by chemical signatures with positive contribution of Sb, Bi, and negative contribution of Ag, Fe, Pb in PLS-DA (Figs. 8 and 12). One interpretation for gold in fractures would involve gold remobilization from the host sulfide minerals and precipitating veinlets within or nearby the parent mineral by fluid infiltration during later hydrothermal events or higher grade metamorphism (Large et al., 2007, 2009; Thomas et al., 2011; Cook et al., 2013; Gao et al., 2015; Larocque et al., 1995; Rezeau et al., 2017). Gold in fractures has been interpreted to be mobilized from oscillatory zoned and fractured auriferous sulfide minerals in different metamorphosed orogenic and Au-rich VMS deposits (Huston et al., 1992; Velásquez et al., 2014; Fougerouse et al., 2016; Hastie et al., 2020). Our study cannot distinguish between remobilized gold and new gold influx during successive hydrothermal stages. Nevertheless, the distinct chemical signatures recognized by PLS-DA from the two gold textures indicates a change in fluid compositions and/or temperatures. The lower Ag content in gold in fractures has been recognized at the Lac Herbin deposit, where the later, higher temperature, Ca-rich, high salinity fluid, precipitated gold in fractures (Rezeau et al., 2017). Therefore, the differences in chemical signatures in gold are likely linked with the changes of fluid composition between different paragenetic events.

4.5. Native gold composition in relation to host rocks

The hydrothermal fluids that form orogenic gold deposits are most likely to have interacted continuously with crustal rocks along the fluid pathways (Garofalo et al., 2014; Goldfarb and Groves, 2015). Thus, modification of a common hydrothermal fluid by local fluid-rock reactions is a likely hypothesis to explain native gold chemistry with respect to the country rock compositions (Fig. 9). Differences in the budget of metals mobilized in metamorphosed orogenic deposits are dominantly controlled by the primary protolith composition and the efficiency of metal mobilization (Pitcairn et al., 2015). Gold in deposits hosted by metasedimentary rocks is characterized by high Ag, Cu, Pb, Hg, but low Fe, Pd, Sb, Bi, which is consistent with the finding that Hg, Pb, and Cu can be released during prograde metamorphism of pyrite in metasedimentary rocks (Large et al., 2007, 2011). Gold in deposits hosted by ultramafic–mafic rocks (e.g., Tarmoola and Cuiaba) are characterized by high Sb probably because Sb can be enriched as the fluids reacted with the host mafic volcanic rocks. The mobilization of Sb during the circulation of metal-rich fluids with host ultramafic rocks has been reported at the Hemlo Au-Mo deposit (Schandl and Gorton, 2000). Gold in deposits hosted by felsic rocks (e.g., Empire and Wulong) has relatively high Pb contents probably because of fluid reaction with felsic rocks. Therefore, the compositions of host rocks exert a control on the trace element content of fluids that precipitated gold, likely as a result of reaction and exchange between hydrothermal fluids and host rocks (Ridley, 2000).

To apply gold compositions as indicators to discriminant host rock types, a dataset of gold compositions from Hollinger, Mclntyre, and Aunor orogenic gold deposits (Canada, Velasquez, 2014), was projected on the latent variable spaces defined by PLS-DA of gold compositions from studied orogenic deposits (Fig. 13). Hollinger and Mclntyre deposits are mainly hosted by metamorphosed mafic lavas and felsic tuffs, whereas the Aunor deposit is hosted by tuffaceous basalts (Bateman et al., 2008; Velasquez, 2014). These gold grains hosted by mafic igneous rocks, form a cluster, with a high proportion of gold grains projected within the ultramafic–mafic region (Fig. 13B). Thus, the results exemplify that trace elements Ag, Cu, Pd, Sb, and Hg have high potential to discriminate gold grains hosted in different country rock types in provenance studies and provide indications in exploration for

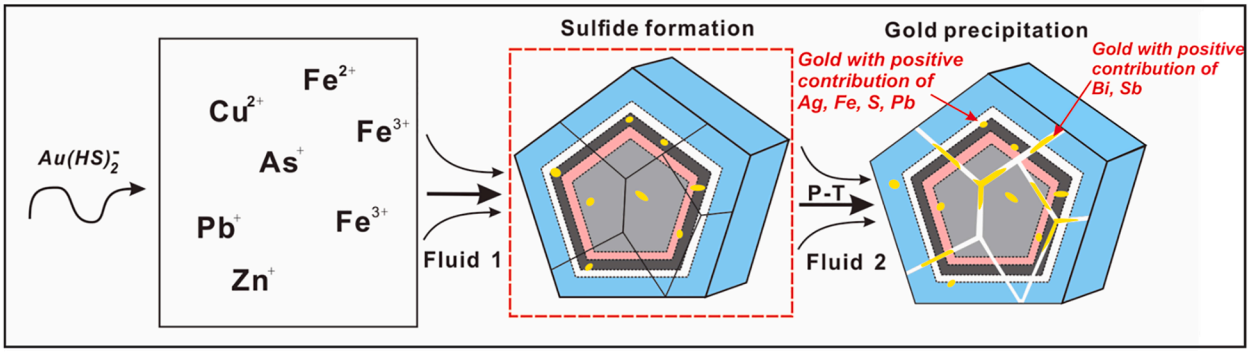

Fig. 12. Schematic summary diagram of native gold in different textures with various trace element compositions. Zoned composition of sulfide minerals refers to Cook et al. (2013), Gao et al. (2015), Large et al. (2009), Large et al. (2007), and Thomas et al. (2011).

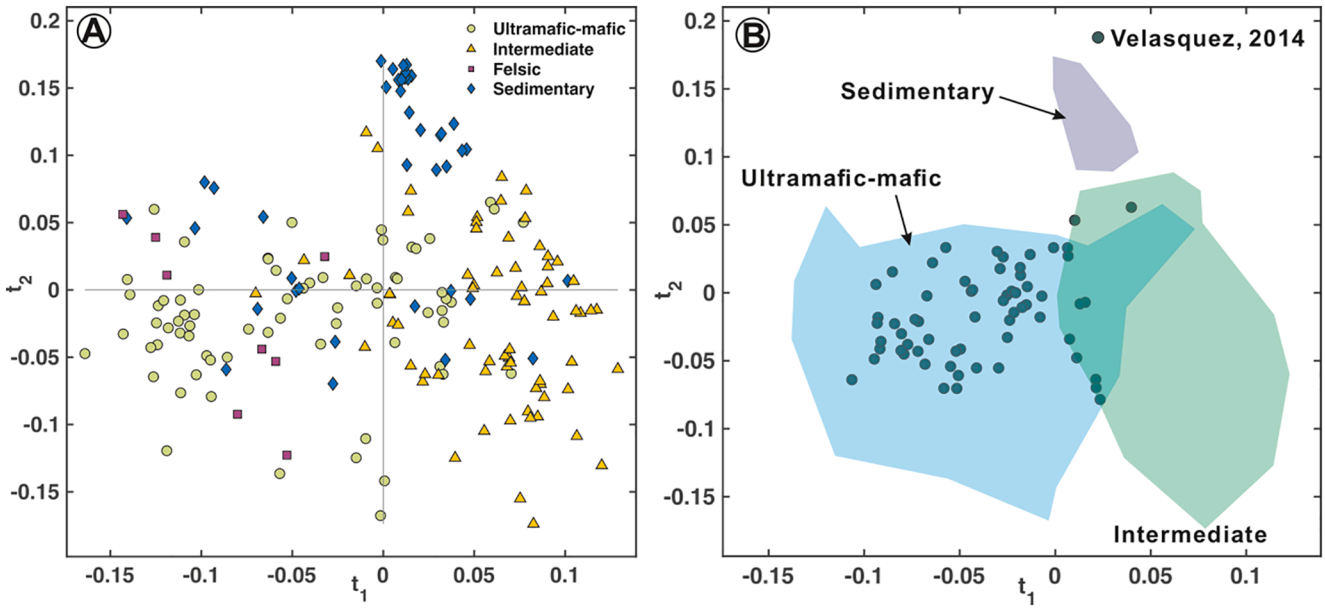

Fig. 13. Application of gold compositions as indicators to fingerprint the host rock types. (A) The first and second scores plot (**t1-t2**) shows the distribution of gold analyses classified by dominant host rocks from studied orogenic gold deposits in the latent variable space defined by loadings (**qw*$_1$-qw*$_2$**). (B) Projection of the compositional data of gold grains from Hollinger, Mclntyre, and Aunor orogenic gold deposits (Canada, Velasquez, 2014).

orogenic gold deposits.

5. Conclusions

Our scoping study shows that major and trace element signatures of native gold from twenty-seven orogenic gold deposits enable discrimination between populations of gold grains in relation to different mineral associations, textures, and dominant country rocks.

Minor elements, such as Ag and Cu, occur in solid solution in gold, whereas elements such as Fe, As, S, Hg, form impurities or micro inclusions due to lattice distortion caused by differences in Ag and Au ionic radius in native gold. The common sulfide inclusion suite (Fe-As-Sb-S) in micro size is the characteristic of native gold from the studied orogenic deposits. Gold grains from orogenic deposits in spatial association with the pyrite-arsenopyrite-chalcopyrite-pyrrhotite-tourmaline assemblage, can be discriminated by PLS-DA based on contributions of Fe, Cu, Pb, Sb, Bi, and Hg. The controls of mineral associations on gold compositions can be explained by partitioning of trace elements between different co-crystallizing minerals and gold during precipitation. Two common types of native gold textures are identified within studied orogenic gold deposits, which are gold inclusions and veinlets. Silver, Fe, Pb, and Bi are the most important elements for distinguishing the compositions of gold related with these two textures. The distinct compositional characteristics of gold inclusions and veinlets result from changes of fluid composition and perhaps fluid temperature. The chemical signatures identified in gold from deposits hosted in different dominant country rocks are probably linked to the primary protolith composition and modification of common metamorphic fluids by local fluid-rock reactions along the flow path. Finally, the statistical models enable comparison of orogenic gold composition to literature data.

Declaration of Competing Interest

The authors declare that they have no known competing financial interests or personal relationships that could have appeared to influence the work reported in this paper.

Acknowledgments

This study was funded by the Natural Science and Engineering Research Council of Canada (NSERC), Agnico Eagle Mines Limited, Ministère de l'Énergie et des Ressources Naturelles du Québec and China Scholarship Council (CSC). We thank Dr. Marc Choquette (U. LAVAL) for his assistance with EPMA, Dr. Zhaoping Yang (GSC) and Mr. Brandon Boucher (UNB) for assistances with LA-ICP-MS. Special thanks to Donald Grzela (Monarques Gold Corporation), Marjorie Sciuba (U. LAVAL), Olivier Côté-Mantha (Agnico Eagle Mines Limited), Junfeng Shen (CUGB), Rodrigo Martins (Anglo Gold Ashanti), and Anthony Pochon (BRGM), who provided representative gold samples for analysis. We also acknowledge constructive comments and suggestions from Dr. David Banks, Dr. Leonid Danyushevsky and an anonymous reviewer and editorial handling by Dr. Franco Pirajno and Dr. Alain Chauvet.

Appendix A. Supplementary data

Supplementary data to this article can be found online at https://doi.org/10.1016/j.oregeorev.2021.104061.

References

Aitchison, J. (1986) The statistical analysis ofcompositional data. Monographs on Statistics and Applied Probability. Chapman and Hall Ltd. Reprinted 2003 with additional material by The Blackburn Press, London (UK) (416 pp.).

Aitchison, J., Greenacre, M., 2002. Biplots of compositional data. J. Roy. Stat. Soc.: Ser. C (Appl. Stat.) 51, 375–392.

Alpers, C.N., Myers, P.A., Millsap, D., Regnier, T.B., 2014. Arsenic associated with historical gold mining in the Sierra Nevada foothills: case study and field trip guide for Empire Mine State Historic Park, California. Rev. Mineral. Geochem. 79, 553–587.

Antweiler, J., Campbell, W., 1977. Application of gold compositional analyses to mineral exploration in the United States. Develop. Econ. Geol. Elsevier 17–29.

Ashley, P., Creagh, C., Ryan, C., 2000. Invisible gold in ore and mineral concentrates from the Hillgrove gold-antimony deposits, NSW, Australia. Miner. Deposita 35, 285–301.

Augustin, J., Gaboury, D., 2019. Multi-stage and multi-sourced fluid and gold in the formation of orogenic gold deposits in the world-class Mana district of Burkina Faso-Revealed by LA-ICP-MS analysis of pyrites and arsenopyrites. Ore Geol. Rev. 104, 495–521.

Banks, D., Chapman, R., Spence-Jones, C., 2018. Detrital gold as a deposit-specific indicator mineral by LA-ICP-MS analysis. Geoscience BC Report 21.

Barker, M., Rayens, W., 2003. Partial least squares for discrimination. J. Chemom. 17, 166–173.
Bateman, R., Ayer, J., Dubé, B., 2008. The Timmins-Porcupine gold camp, Ontario: Anatomy of an Archean greenstone belt and ontogeny of gold mineralization. Econ. Geol. 103, 1285–1308.
Billay, A., Kisters, A., Meyer, F., Schneider, J., 1997. The geology of the Lega Dembi gold deposit, southern Ethiopia: implications for Pan-African gold exploration. Miner. Deposita 32, 491–504.
Bogatu, A. (2017) The orfée prospect: a neoarchean orogenic gold occurrence along the contact between the La Grande and Opinaca subprovinces (Eeyou Istchee James Bay, Québec). MSc dissertation, Université Laval.
Boyle, R.W. (1979) The geochmistry of gold and its deposits. Geol. Surv. Can. Bull. 280.
Brereton, R.G., Lloyd, G.R., 2014. Partial least squares discriminant analysis: taking the magic away. J. Chemom. 28, 213–225.
Carpenter, R.L., Duke, N.A., Sandeman, H.A., Stern, R., 2005. Relative and absolute timing of gold mineralization along the Meliadine trend, Nunavut, Canada: evidence for Paleoproterozoic gold hosted in an Archean greenstone belt. Econ. Geol. 100, 567–576.
Cave, B.J., Barnes, S.-J., Pitcairn, I.K., Sack, P.J., Kuikka, H., Johnson, S.C., Duran, C.J., 2019. Multi-stage precipitation and redistribution of gold, and its collection by lead-bismuth and lead immiscible liquids in a reduced-intrusion related gold system (RIRGS); Dublin Gulch, western Canada. Ore Geol. Rev. 106, 28–55.
Chapman, R., Leake, R., Bond, D., Stedra, V., Fairgrieve, B., 2009. Chemical and mineralogical signatures of gold formed in oxidizing chloride hydrothermal systems and their significance within populations of placer gold grains collected during reconnaissance. Econ. Geol. 104, 563–585.
Chapman, R., Mileham, T., Allan, M., Mortensen, J., 2017. A distinctive Pd-Hg signature in detrital gold derived from alkalic Cu-Au porphyry systems. Ore Geol. Rev. 83, 84–102.
Chapman, R., Mortensen, J., Crawford, E., LeBarge, W., 2010a. Microchemical studies of placer and lode gold in the Klondike District, Yukon, Canada: 1. Evidence for a small, gold-rich, orogenic hydrothermal system in the Bonanza and Eldorado Creek area. Econ. Geol. 105, 1369–1392.
Chapman, R., Mortensen, J., Crawford, E., Lebarge, W., 2010b. Microchemical studies of placer and lode gold in the Klondike District, Yukon, Canada: 2. Constraints on the nature and location of regional lode sources. Econ. Geol. 105, 1393–1410.
Chapman, R., Shaw, M., Leake, R., Jackson, B., 2005. Gold in the Central Ochil Hills, Scotland. Trans Inst Min Metall B Appl Earth Sci 114, 53–64.
Chapman, R.J., Allan, M.M., Mortensen, J.K., Wrighton, T.M., Grimshaw, M.R., 2018. A new indicator mineral methodology based on a generic Bi-Pb-Te-S mineral inclusion signature in detrital gold from porphyry and low/intermediate sulfidation epithermal environments in Yukon Territory, Canada. Miner. Deposita 53, 815–834.
Chapman, R.J., Mortensen, J.K., 2016. Characterization of Gold Mineralization in the Northern Cariboo Gold District, British Columbia, Canada, Through Integration of Compositional Studies of Lode and Detrital Gold with Historical Placer Production: A Template for Evaluation of Orogenic Gold Districts. Econ. Geol. 111, 1321–1345.
Chapman, R.J., Mortensen, J.K., LeBarge, W.P., 2011. Styles of lode gold mineralization contributing to the placers of the Indian River and Black Hills Creek, Yukon Territory, Canada as deduced from microchemical characterization of placer gold grains. Miner. Deposita 46, 881–903.
Chouinard, A., Williams-Jones, A.E., Leonardson, R.W., Hodgson, C.J., Silva, P., Téllez, C., Vega, J., Rojas, F., 2005. Geology and genesis of the multistage high-sulfidation epithermal Pascua Au-Ag-Cu deposit, Chile and Argentina. Econ. Geol. 100, 463–490.
Chudnenko, K.V., Palyanova, G.A., 2016. Thermodynamic modeling of native formation of Au–Ag–Cu–Hg solid solutions. Appl. Geochem. 66, 88–100.
Cook, N.J., Ciobanu, C.L., Meria, D., Silcock, D., Wade, B., 2013. Arsenopyrite-pyrite association in an orogenic gold ore: tracing mineralization history from textures and trace elements. Econ. Geol. 108, 1273–1283.
Cooke, D.R., Wilkinson, J.J., Baker, M., Agnew, P., Phillips, J., Chang, Z., Chen, H., Wilkinson, C.C., Inglis, S., Hollings, P. (2020) Using Mineral Chemistry to Aid Exploration: A Case Study from the Resolution Porphyry Cu-Mo Deposit, Arizona. Economic Geology doi:10.5382/econgeo.4735; 28 p.
Côté-Mantha, O., Gosselin, G., Vaillancourt, D., Blackburn, A. (2017) The Amaruq Deposits – Building a Customized Toolset and Using a Flexible Geomodel: Optimization from Discovery to Mine Development. 553-567.
Cox, S., Ruming, K., 2004. The St Ives mesothermal gold system, Western Australia—a case of golden aftershocks? J. Struct. Geol. 26, 1109–1125.
Cracknell, M.J., Baker, M.J., Cooke, D.R., Escolme, A. (2019) Multielement geochemical data missing value and below detection limit imputation, SEG 2019 Conference, pp. 1-2.
Crawford, E.C., 2007. Klondike placer gold: New tools for examining morphology, composition and crystallinity. MSc dissertation. University of British Columbia.
Daigneault, R., Mueller, W., Chown, E., 2002. Oblique Archean subduction: accretion and exhumation of an oceanic arc during dextral transpression, Southern Volcanic Zone, Abitibi Subprovince Canada. Precambr. Res. 115, 261–290.
Daoust, C., Voicu, G., Brisson, H., Gauthier, M., 2011. Geological setting of the Paleoproterozoic Rosebel gold district, Guiana Shield, Suriname. J. S. Am. Earth Sci. 32, 222–245.
Daver, L.M., Jébrak, M., Beaudoin, G., Trumbull, R.B. (2020) Three-stage formation of greenstone-hosted orogenic gold deposits in the val-d'or mining district, abitibi, canada: evidence from pyrite and tourmaline. Ore Geology Reviews: 103449.
Bronac, D.e., de Vazelhes, V., 2019. Étude de la dispersion d'un gisement d'or dans les sédiments glaciaires: le cas d'Amaruq. MSc dissertation. Université Laval, (Nunavut, Canada).
Desborough, G.A., 1970. Silver depletion indicated by microanalysis of gold from placer occurrences, western United States. Econ. Geol. 65, 304–311.
Dmitrijeva, M., Ciobanu, C.L., Ehrig, K.J., Cook, N.J., Metcalfe, A.V., Verdugo-Ihl, M.R., McPhie, J., 2019. Mineralization-alteration footprints in the Olympic Dam IOCG district, South Australia: the Acropolis prospect. J. Geochem. Explor. 205, 106333.
Dubé, B., Gosselin, P. (2007) Greenstone-hosted quartz-carbonate vein deposits. Geological Association of Canada, Mineral Deposits Division: 49-73.
Duuring, P., Hagemann, S.G., Cassidy, K.F., Johnson, C.A., 2004. Hydrothermal alteration, ore fluid characteristics, and gold depositional processes along a trondhjemite-komatiite contact at Tarmoola, Western Australia. Econ. Geol. 99, 423–451.
Dvorani, S.N., 2016. Solid Inclusions in Au-nuggets, genesis and derivation from alkaline rocks of the Guli Massif, Northern Siberia. Open Geosciences 8, 195–213.
Eilu, P., Sorjonen-Ward, P., Nurmi, P., Niiranen, T., 2003. A review of gold mineralization styles in Finland. Econ. Geol. 98, 1329–1353.
Eriksson, L., Byrne, T., Johansson, E., Trygg, J., Vikström, C., 2013. Multi-and megavariate data analysis basic principles and applications. Umetrics Academy.
Eriksson, L., Johansson, E., Kettaneh-Wold, N., Wold, S., 2001. Multi-and megavariate data analysis: principles and applications. Umetrics.
Fang, X., Tang, J., Beaudoin, G., Song, Y., Chen, Y., 2020. Geology, mineralogy and geochemistry of the Shangxu orogenic gold deposit, central Tibet, China: implications for mineral exploration. Ore Geol. Rev. 103440.
Fleet, M.E., Mumin, A.H., 1997. Gold-bearing arsenian pyrite and marcasite and arsenopyrite from Carlin Trend gold deposits and laboratory synthesis. Am. Mineral. 82, 182–193.
Fougerouse, D., Micklethwaite, S., Tomkins, A.G., Mei, Y., Kilburn, M., Guagliardo, P., Fisher, L.A., Halfpenny, A., Gee, M., Paterson, D., 2016. Gold remobilisation and formation of high grade ore shoots driven by dissolution-reprecipitation replacement and Ni substitution into auriferous arsenopyrite. Geochim. Cosmochim. Acta 178, 143–159.
Frimmel, H.E. (2014) A giant mesoarchean crustal gold-enrichment episode: possible causes and consequences for exploration. doi: 10.1.1.722.1449.
Gaboury, D., 2019. Parameters for the formation of orogenic gold deposits. Appl. Earth Sci. 1–10.
Gammons, C., Yu, Y., Bloom, M., 1993. Experimental investigation of the hydrothermal geochemistry of platinum and palladium: III. The solubility of Ag-Pd alloy+ AgCl in NaCl/HCl solutions at 300 C. Geochim. Cosmochim. Acta 57, 2469–2479.
Gammons, C.H., Williams-Jones, A., 1995. The solubility of Au Ag alloy+ AgCl in HCl/NaCl solutions at 300° C: New data on the stability of Au (1) chloride complexes in hydrothermal fluids. Geochim. Cosmochim. Acta 59, 3453–3468.
Gao, J., Jackson, S., Dubé, B., Kontak, D., De Souza, S., Dubé, B., Mercier-Langevin, P., 2015. Genesis of the Canadian Malartic, Côté Gold, and Musselwhite gold deposits: Insights from LA-ICP-MS element mapping of pyrite. Targeted geoscience initiative 4, 157–175.
Garofalo, P.S., Fricker, M.B., Günther, D., Bersani, D., Lottici, P.P., 2014. Physical-chemical properties and metal budget of Au-transporting hydrothermal fluids in orogenic deposits. Geological Society, London, Special Publications 402, 71–102.
Gas'kov, I., 2017. Major impurity elements in native gold and their association with gold mineralization settings in deposits of Asian folded areas. Russ. Geol. Geophys. 58, 1080–1092.
George, L.L., Cook, N.J., Crowe, B.B., Ciobanu, C.L., 2018. Trace elements in hydrothermal chalcopyrite. Mineral. Mag. 82, 59–88.
Gilbert, S., Danyushevsky, L., Goemann, K., Death, D., 2014. Fractionation of sulphur relative to iron during laser ablation-ICP-MS analyses of sulphide minerals: implications for quantification. J. Anal. At. Spectrom. 29, 1024–1033.
Goldfarb, R., Baker, T., Dube, B., Groves, D.I., Hart, C.J., Gosselin, P. (2005) Distribution, character and genesis of gold deposits in metamorphic terranes. Economic geology 100th Anniversary volume. Society of Economic Geologists, Littleton, Colorado, USA.
Goldfarb, R., Groves, D., Gardoll, S., 2001. Orogenic gold and geologic time: a global synthesis. Ore Geol. Rev. 18, 1–75.
Goldfarb, R.J., Groves, D.I., 2015. Orogenic gold: common or evolving fluid and metal sources through time. Lithos 233, 2–26.
Groves, D.I., Goldfarb, R.J., Robert, F., Hart, C.J., 2003. Gold deposits in metamorphic belts: overview of current understanding, outstanding problems, future research, and exploration significance. Econ. Geol. 98, 1–29.
Grunsky, E., Caritat, P.d. (2017) Advances in the use of geochemical data for mineral exploration, Proceedings of exploration, pp. 441-456.
Grunsky, E., de Caritat, P., 2020. State-of-the-art analysis of geochemical data for mineral exploration. Geochemistry: Exploration. Environment, Analysis 20, 217–232.
Grunsky, E.C., 2010. The interpretation of geochemical survey data. Geochemistry: Exploration. Environment, Analysis 10, 27–74.
Hanes, R., Huot, F., Cleven, N.R., Goutier, J., Beaudoin, G., Guilmette, C. (2017) Orogenic gold veins related to transpressional shear zones along the north-western contact of the La Grande and Opinaca subprovinces, Eeyou Istchee James Bay, Québec, Canada, Proceedings of the 14th Biennial SGA Meeting, vol 1. Society for Geology Applied to Mineral Deposits, pp. 39-42.
Hastie, E.C., Kontak, D.J., Lafrance, B., 2020. Gold Remobilization: insights from Gold Deposits in the Archean Swayze Greenstone Belt, Abitibi Subprovince, Canada. Econ. Geol. 115, 241–277.
Hough, R.M., Butt, C.R.M., Fischer-Buhner, J., 2009. The Crystallography, Metallography and Composition of Gold. Elements 5, 297–302.
Hron, K., Tempi, M., Filzmoser, P. (2010) Exploratory compositional data analysis using the R-package robCompositions.

Huang, X.-W., Boutroy, É., Makvandi, S., Beaudoin, G., Corriveau, L., De Toni, A.F., 2019a. Trace element composition of iron oxides from IOCG and IOA deposits: relationship to hydrothermal alteration and deposit subtypes. Miner. Deposita 54, 525–552.

Huang, X.-W., Sappin, A.-A., Boutroy, É., Beaudoin, G., Makvandi, S. (2019b) Trace Element Composition of Igneous and Hydrothermal Magnetite from Porphyry Deposits: Relationship to Deposit Subtypes and Magmatic Affinity. Economic Geology 114: 917-952.

Huston, D.L., Bottrill, R.S., Creelman, R.A., Zaw, K., Ramsden, T.R., Rand, S.W., Gemmell, J.B., Jablonski, W., Sie, S., Large, R.R., 1992. Geologic and geochemical controls on the mineralogy and grain size of gold-bearing phases, eastern Australian volcanic-hosted massive sulfide deposits. Econ. Geol. 87, 542–563.

Jackson, S.E., Sylvester, P., 2008. Calibration strategies for elemental analysis by LA-ICP-MS. Signal 10 (1000), 100.

Jochum, K.P., Nohl, U., Herwig, K., Lammel, E., Stoll, B., Hofmann, A.W., 2005. GeoReM: a new geochemical database for reference materials and isotopic standards. Geostand. Geoanal. Res. 29, 333–338.

Junhao, W., Xiaoping, Q., Dazhao, G., Wenjuan, T., 2004. Geochemistry of Ore Fluids and Rb-Sr Isotopic Dating for the Wulong Gold Deposit in Liaoning, China. Acta Geologica Sinica (English Edition) 78, 1267–1274.

Kalliomäki, H., Wagner, T., Fusswinkel, T., Sakellaris, G., 2017. Major and trace element geochemistry of tourmalines from Archean orogenic gold deposits: proxies for the origin of gold mineralizing fluids? Ore Geol. Rev. 91, 906–927.

Knight, J., Mortensen, J., Morison, S., 1999. Lode and placer gold composition in the Klondike District, Yukon Territory, Canada; implications for the nature and genesis of Klondike placer and lode gold deposits. Econ. Geol. 94, 649–664.

Large, R.R., Bull, S.W., Maslennikov, V.V., 2011. A carbonaceous sedimentary source-rock model for Carlin-type and orogenic gold deposits. Econ. Geol. 106, 331–358.

Large, R.R., Danyushevsky, L., Hollit, C., Maslennikov, V., Meffre, S., Gilbert, S., Bull, S., Scott, R., Emsbo, P., Thomas, H., 2009. Gold and trace element zonation in pyrite using a laser imaging technique: implications for the timing of gold in orogenic and Carlin-style sediment-hosted deposits. Econ. Geol. 104, 635–668.

Large, R.R., Maslennikov, V.V., Robert, F.o., Danyushevsky, L.V., Chang, Z. (2007) Multistage sedimentary and metamorphic origin of pyrite and gold in the giant Sukhoi Log deposit, Lena gold province, Russia. Economic Geology 102: 1233-1267.

Larocque, A.C., Hodgson, C.J., Cabri, L.J., Jackman, J.A., 1995. Ion-microprobe analysis of pyrite, chalcopyrite and pyrrhotite from the Mobrun VMS deposit in northwestern Quebec; evidence for metamorphic remobilization of gold. Canad. Mineral. 33, 373–388.

Laverov, N., Lishnevskii, E., Distler, V., Chernov, A. (2000) Model of the ore-magmatic system of the Sukhoi Log gold-platinum deposit, Eastern Siberia, Russia, Doklady Earth Sciences. Pleiades Publishing, Ltd.(Плеадес Паблишинг, Лтд), pp. 1362-1365.

Lawley, C.J.M., Dubé, B., Mercier-Langevin, P., Kjarsgaard, B., Knight, R., Vaillancourt, D., 2015. Defining and mapping hydrothermal footprints at the BIF-hosted Meliadine gold district, Nunavut, Canada. J. Geochem. Explor. 155, 33–55.

Longerich, H., Jackson, S., Gunther, D. (1996) Laser ablation inductively coupled plasma mass spectrometric transient signal data acquisition and analyte concentration calculation (vol 11, pg 899, 1996). Royal Soc Chemistry Thomas Graham House, Science Park, Milton Road, Cambridge, Cambs, England, pp. 391-391.

Makvandi, S., Ghasemzadeh-Barvarz, M., Beaudoin, G., Grunsky, E.C., McClenaghan, M. B., Duchesne, C., Boutroy, E., 2016. Partial least squares-discriminant analysis of trace element compositions of magnetite from various VMS deposit subtypes: application to mineral exploration. Ore Geol. Rev. 78, 388–408.

McClenaghan, M.B., 2005. Indicator mineral methods in mineral exploration. Geochem. Explor. Environ. Anal. 5, 233–245.

McClenaghan, M.B., 2011. Overview of common processing methods for recovery of indicator minerals from sediment and bedrock in mineral exploration. Geochem. Explor. Environ. Anal. 11, 265–278.

McClenaghan, M.B., Layton-Matthews, D., 2017. Application of indicator mineral methods to bedrock and sediments. Geological Survey of Canada Open File 8345, 90 p. https://doi.org/10.4095/306305.

Meffre, S., Large, R.R., Scott, R., Woodhead, J., Chang, Z., Gilbert, S.E., Danyushevsky, L. V., Maslennikov, V., Hergt, J.M., 2008. Age and pyrite Pb-isotopic composition of the giant Sukhoi Log sediment-hosted gold deposit, Russia. Geochim. Cosmochim. Acta 72, 2377–2391.

Meffre, S., Large, R.R., Steadman, J.A., Gregory, D.D., Stepanov, A.S., Kamenetsky, V.S., Ehrig, K., Scott, R.J., 2016. Multi-stage enrichment processes for large gold-bearing ore deposits. Ore Geol. Rev. 76, 268–279.

Mehrabi, B., Karimishahraki, B., Banks, D., Boyce, A., Yardley, B.W., 2019. Hydrothermal iron oxide-Cu-Au (IOCG) mineralization at the Jalal-Abad deposit, northwestern Zarand, Iran. Ore Geol. Rev. 106, 300–317.

Mercier-Langevin, P., Daigneault, R., Goutier, J., Dion, C., Archer, P., 2012. Geology of the Archean Intrusion-Hosted La-Grande-Sud Au-Cu Prospect, La Grande Subprovince, James Bay Region, Quebec. Econ. Geol. 107, 935–962.

Mernagh, T.P., 2001. A fluid inclusion study of the Fosterville Mine: a turbidite-hosted gold field in the Western Lachlan Fold Belt, Victoria, Australia. Chem. Geol. 173, 91–106.

Michibayashi, K., 1995. Two phase syntectonic gold mineralization and barite remobilization within the main ore body of the Golden Giant mine, Hemlo, Ontario, Canada. Ore Geol. Rev. 10, 31–50.

Milidragovic, D., Beaudoin, G., Jackson, S. (2016) In-situ trace element characterization of three gold reference materials using EPMA and LA-ICP-MS. Geological Survey of Canada. Open File 8096, 1.zip file. https://doi.org/10.4095/299097.

Moles, N., Chapman, R., Warner, R., 2013. The significance of copper concentrations in natural gold alloy for reconnaissance exploration and understanding gold-depositing hydrothermal systems. Geochem. Explor. Environ. Anal. 13, 115–130.

Morrison, G.W., Rose, W.J., Jaireth, S., 1991. Geological and geochemical controls on the silver content (fineness) of gold in gold-silver deposits. Ore Geol. Rev. 6, 333–364.

Mosier, E.L., Cathrall, J.B., Antweiler, J.C., Tripp, R.B., 1989. Geochemistry of placer gold, Koyukuk-Chandalar mining district, Alaska. J. Geochem. Explor. 31, 97–115.

Mountain, B., Seward, T., 2003. Hydrosulfide/sulfide complexes of copper (I): experimental confirmation of the stoichiometry and stability of Cu (HS) 2− to elevated temperatures. Geochim. Cosmochim. Acta 67, 3005–3014.

Nguimatsia Dongmo, F.W., Chapman, R.J., Bolarinwa, A.T., Yongue, R.F., Banks, D.A., Olajide-Kayode, J.O., 2019. Microchemical characterization of placer gold grains from the Meyos-Essabikoula area, Ntem complex, southern Cameroon. J. Afr. Earth Sc. 151, 189–201.

Nysten, P., 1986. Gold in the volcanogenic mercury-rich sulfide deposit Långsele, Skellefte ore district, northern Sweden. Miner. Deposita 21, 116–120.

Omang, B., Suh, C., Lehmann, B., Vishiti, A., Chombong, N., Fon, A., Egbe, J., Shemang, E., 2015. Microchemical signature of alluvial gold from two contrasting terrains in Cameroon. J. Afr. Earth Sc. 112, 1–14.

Pal'yanova, G., 2008. Physicochemical modeling of the coupled behavior of gold and silver in hydrothermal processes: gold fineness, Au/Ag ratios and their possible implications. Chem. Geol. 255, 399–413.

Palarea-Albaladejo, J., Martín-Fernández, J.A., 2015. zCompositions—R package for multivariate imputation of left-censored data under a compositional approach. Chemometrics and intelligent laboratory systems 143, 85–96.

Palarea-Albaladejo, J., Martín-Fernández, J.A., Buccianti, A., 2014. Compositional methods for estimating elemental concentrations below the limit of detection in practice using R. J. Geochem. Explor. 141, 71–77.

Palarea-Albaladejo, J., Martín-Fernández, J.A., Gómez-García, J., 2007. A parametric approach for dealing with compositional rounded zeros. Math. Geol. 39, 625–645.

Paton, C., Hellstrom, J., Paul, B., Woodhead, J., Hergt, J., 2011. Iolite: Freeware for the visualisation and processing of mass spectrometric data. J. Anal. At. Spectrom. 26, 2508–2518.

Pearcy, E.C., Petersen, U., 1990. Mineralogy, geochemistry and alteration of the Cherry Hill, California hot-spring gold deposit. J. Geochem. Explor. 36, 143–169.

Pilote, P. (2000) Géologie de la région de Val-d'Or, Sous-province d'Abitibi. Ministère des Ressources naturelles du Québec. MB-2000-09.

Pitcairn, I.K., Craw, D., Teagle, D.A., 2015. Metabasalts as sources of metals in orogenic gold deposits. Miner. Deposita 50, 373–390.

Pochon, A., Gapais, D., Gloaguen, E., Gumiaux, C., Branquet, Y., Cagnard, F., Martelet, G., 2016. Antimony deposits in the Variscan Armorican belt, a link with mafic intrusives? Terra Nova 28, 138–145.

Pochon, A., Gapais, D., Gumiaux, C., Branquet, Y., Gloaguen, E., Cagnard, F., Martelet, G. (2015) Sb-Deposits in the Variscan Armorican Belt (France)-Potential Relationships with Basic Intrusions and High-Density Magnetic Lithologies at Depth, SGA2015: 13th Biennial meeting, pp. 831-834.

Pokrovski, G., Kokh, M., Proux, O., Hazemann, J.-L., Bazarkina, E., Testemale, D., Escoda, C., Boiron, M.-C., Blanchard, M., Aigouy, T., 2019. The nature and partitioning of invisible gold in the pyrite-fluid system. Ore Geol. Rev. 109, 545–563.

Potter, M., Styles, M., 2003. Gold characterisation as a guide to bedrock sources for the Estero Hondo alluvial gold mine, western Ecuador. Applied Earth Science: Transactions of the Institutions of Mining and Metallurgy: Section B 112, 297–304.

Poulsen, K.H., 2000. Geological classification of Canadian gold deposits. Bulletin of the Geological Survey of Canada 540, 1–106.

Railsback, L.B., 2003. An earth scientist's periodic table of the elements and their ions. Geology 31, 737–740.

Raynor, G.V., 1976. The alloying behaviour of gold. Gold Bull. 9, 12–19.

Rezeau, H., Moritz, R., Beaudoin, G., 2017. Formation of Archean batholith-hosted gold veins at the Lac Herbin deposit, Val-d'Or district, Canada: Mineralogical and fluid inclusion constraints. Miner. Deposita 52, 421–442.

Ribeiro-Rodrigues, L.C., de Oliveira, C.G., Friedrich, G., 2007. The Archean BIF-hosted Cuiabá Gold deposit, Quadrilátero Ferrífero, Minas Gerais, Brazil. Ore Geol. Rev. 32, 543–570.

Ridley, J.R., 2000. Fluid chemistry of orogenic lode deposits and implications for genetic models. Rev. Econ. Geol. 13, 141–162.

Robert, F., Poulsen, K., Dubé, B., 1997. Gold deposits and their geological classification. Proceedings of Exploration 209–220.

Rocholl, A.B., Simon, K., Jochum, K.P., Bruhn, F., Gehann, R., Kramar, U., Luecke, W., Molzahn, M., Pernicka, E., Seufert, M., 1997. Chemical Characterisation of NIST Silicate Glass Certified Reference Material SRM 610 by ICP-MS, TIMS, LIMS, SSMS, INAA, AAS and PIXE. Geostandards Newsletter 21, 101–114.

Roussy, J. (2004) Relations entre la distribution de l'or, la structure, la composition des veines et de l'alteration hydrothermale a la Mine Beaufor, Val-d'Or, Abitibi, Quebec (French text).

Rushton, R., Nesbitt, B., Muehlenbachs, K., Mortensen, J.K., 1993. A fluid inclusion and stable isotope study of Au quartz veins in the Klondike District, Yukon Territory, Canada; a section through a mesothermal vein system. Econ. Geol. 88, 647–678.

Sammelin, M., Wanhainen, C., Martinsson, O., 2011. Gold mineralogy at the Aitik Cu–Au–Ag deposit, Gällivare area, northern Sweden. Gff 133, 19–30.

Schandl, E.S., Gorton, M.P., 2000. Sb-enriched ultramafic lamprophyre in the Hemlo Au-Mo deposit of the Superior Province, Canada: evidence for post-Archean Sb mobility. Eur. J. Mineral. 12, 625–637.

Sciuba, M., Beaudoin, G., Grzela, D., Makvandi, S., 2020a. Trace element composition of scheelite in orogenic gold deposits. Miner. Deposita 55, 1149–1172.

Sciuba, M., Beaudoin, G., Makvandi, S., 2020b. Chemical composition of tourmaline in orogenic gold deposits. Miner. Deposita. https://doi.org/10.1007/s00126-020-00981-x.

Shelton, K.L., McMenamy, T.A., Hees, E.H.v., Falck, H. (2004) Deciphering the complex fluid history of a greenstone-hosted gold deposit: Fluid inclusion and stable isotope

studies of the Giant mine, Yellowknife, Northwest Territories, Canada. Economic Geology 99: 1643-1663.
Simard, M., Gaboury, D., Daigneault, R., Mercier-Langevin, P., 2013. Multistage gold mineralization at the Lapa mine, Abitibi Subprovince: insights into auriferous hydrothermal and metasomatic processes in the Cadillac-Larder Lake Fault Zone. Miner. Deposita 48, 883–905.
Sylvester, P., Cabri, L., Tubrett, M., McMahon, G., Laflamme, J., Peregoedova, A. (2005) Synthesis and evaluation of a fused pyrrhotite standard reference material for platinum group element and gold analysis by laser ablation-ICPMS, 10th International Platinum Symposium: Oulu, Geological Survey of Finland, Extended Abstracts, pp. 16-20.
Taylor, B.E. (2007) Epithermal gold deposits. Mineral Deposits of Canada: A synthesis of major deposit-types, district metallogeny, the evolution of geological provinces, and exploration methods: Geological Association of Canada, Mineral Deposits Division, Special Publication 5: 113-139.
Thomas, H.V., Large, R.R., Bull, S.W., Maslennikov, V., Berry, R.F., Fraser, R., Froud, S., Moye, R., 2011. Pyrite and pyrrhotite textures and composition in sediments, laminated quartz veins, and reefs at Bendigo gold mine, Australia: insights for ore genesis. Econ. Geol. 106, 1–31.
Tomkins, A.G., Frost, B.R., Pattison, D.R., 2006. Arsenopyrite melting during metamorphism of sulfide ore deposits. The Canadian Mineralogist 44, 1045–1062.
Townley, B.K., Hérail, G., Maksaev, V., Palacios, C., de Parseval, P., Sepulveda, F., Orellana, R., Rivas, P., Ulloa, C., 2003. Gold grain morphology and composition as an exploration tool: application to gold exploration in covered areas. Geochem. Explor. Environ. Analysis 3, 29–38.
Tshibubudze, A., Hein, K.A., 2016. Gold mineralisation in the Essakane goldfield in Burkina Faso, West African craton. Ore Geol. Rev. 78, 652–659.
Valette, M., De Souza, S., Mercier-Langevin, P., McNicoll, V.J., Grondin-LeBlanc, P., Côté-Mantha, O., Simard, M., and Malo, M. (2018) Lithological, hydrothermal, structural and metamorphic controls on the style, geometry and distribution of the auriferous zones at Amaruq, Churchill Province, Nunavut. Targeted Geoscience Initiative: 2017 report of activities, 1: 153-156.
Velasquez, A. (2014) Trace element analysis of native gold by laser ablation ICP-MS: A case study in greenstone-hosted quartz-carbonate vein ore deposits, Timmins, Ontario. MSc dissertation, University of British Columbia.
Velásquez, G., Béziat, D., Salvi, S., Siebenaller, L., Borisova, A.Y., Pokrovski, G.S., De Parseval, P., 2014. Formation and deformation of pyrite and implications for gold mineralization in the El Callao District, Venezuela. Econ. Geol. 109, 457–486.
Wagner, T., Klemd, R., Wenzel, T., Mattsson, B., 2007. Gold upgrading in metamorphosed massive sulfide ore deposits: Direct evidence from laser-ablation–inductively coupled plasma–mass spectrometry analysis of invisible gold. Geology 35, 775–778.
Watling, R.J., Herbert, H.K., Delev, D., Abell, I.D., 1994. Gold fingerprinting by laser ablation inductively coupled plasma mass spectrometry. Spectrochim. Acta, Part B 49, 205–219.
Williams-Jones, A.E., Bowell, R.J., Migdisov, A.A., 2009. Gold in solution. Elements 5, 281–287.
Wilson, S., Ridley, W., Koenig, A., 2002. Development of sulfide calibration standards for the laser ablation inductively-coupled plasma mass spectrometry technique. J. Anal. At. Spectrom. 17, 406–409.
Wyche, N., Eilu, P., Koppström, K., Kortelainen, V., Niiranen, T., Välimaa, J., 2015. The Suurikuusikko gold deposit (Kittilä mine), northern Finland. Mineral Deposits of Finland. Elsevier 411–433.
Wyman, D.A., Cassidy, K.F., Hollings, P., 2016. Orogenic gold and the mineral systems approach: resolving fact, fiction and fantasy. Ore Geol. Rev. 78, 322–335.